UNIVERSITY *of York*

This is a repository copy of *Isoprene chemistry in pristine and polluted Amazon environments:Eulerian and Lagrangian model frameworks and the strong bearing they have on our understanding of surface ozone and predictions of rainforest exposure to this priority pollutant*.

Article:

White Rose
university consortium
Universities of Leeds, Sheffield & York

eprints@whiterose.ac.uk
https://eprints.whiterose.ac.uk/

Atmospheric Chemistry and Physics

Open Access

Discussions

Isoprene chemistry in pristine and polluted Amazon environments: Eulerian and Lagrangian model frameworks and the strong bearing they have on our understanding of surface ozone and predictions of rainforest exposure to this priority pollutant

J. G. Levine[1,2], A. R. MacKenzie[1,2], O. J. Squire[3], A. T. Archibald[3,4],
P. T. Griffiths[3], N. L. Abraham[3,4], J. A. Pyle[3,4], D. E. Oram[5], G. Forster[5],
J. F. Brito[6], J. D. Lee[7], J. R. Hopkins[7], A. C. Lewis[7], S. J. B. Bauguitte[8],
C. F. Demarco[1], P. Artaxo[6], P. Messina[9], J. Lathière[9], D. A. Hauglustaine[9],
E. House[10], C. N. Hewitt[10], and E. Nemitz[11]

[1]School of Geography, Earth and Environmental Sciences, University of Birmingham, Birmingham, UK

[2]Birmingham Institute of Forest Research, University of Birmingham, Birmingham, UK
[3]Centre for Atmospheric Science, University of Cambridge, Cambridge, UK
[4]National Centre for Atmospheric Science, University of Cambridge, Cambridge, UK
[5]National Centre for Atmospheric Science, Centre for Oceanography and Atmospheric Science, School of Environmental Sciences, University of East Anglia, Norwich, UK
[6]Institute of Physics, University of São Paulo, São Paulo, Brazil
[7]National Centre for Atmospheric Science, Department of Chemistry, University of York, UK
[8]Facility for Airborne Atmospheric Measurements, Natural Environment Research Council, Cranfield, UK
[9]Laboratoire des Sciences du Climat et de l'Environnement, IPSL, UVSQ, CEA, CNRS, Gif-sur-Yvette, France
[10]Lancaster Environment Centre, Lancaster University, Lancaster, UK
[11]NERC Centre for Ecology and Hydrology, Edinburgh, Bush Estate, Penicuik, UK

Correspondence to: A. R. MacKenzie (a.r.mackenzie@bham.ac.uk)

Isoprene chemistry in pristine and polluted Amazon environments

J. G. Levine et al.

Title Page

Abstract	Introduction
Conclusions	References
Tables	Figures

⏮   ⏭

◀   ▶

Back   Close

Full Screen / Esc

Printer-friendly Version

Interactive Discussion

Abstract

This study explores our ability to simulate the atmospheric chemistry stemming from isoprene emissions in pristine and polluted regions of the Amazon basin. We confront two atmospheric chemistry models – a global, Eulerian chemistry-climate model (UM-UKCA) and a trajectory-based Lagrangian model (CiTTyCAT) – with recent airborne measurements of atmospheric composition above the Amazon made during the SAMBBA campaign of 2012. The simulations with the two models prove relatively insensitive to the chemical mechanism employed; we explore one based on the Mainz Isoprene Mechanism, and an updated one that includes changes to the chemistry of first generation isoprene nitrates (ISON) and the regeneration of hydroxyl radicals via the formation of hydroperoxy-aldehydes (HPALDS) from hydroperoxy radicals (ISO$_2$). In the Lagrangian model, the impact of increasing the spatial resolution of trace gas emissions employed from $3.75° \times 2.5°$ to $0.1° \times 0.1°$ varies from one flight to another, and from one chemical species to another. What consistently proves highly influential on our simulations, however, is the model framework itself – how the treatment of transport, and consequently mixing, differs between the two models. The lack of explicit mixing in the Lagrangian model yields variability in atmospheric composition more reminiscent of that exhibited by the measurements. In contrast, the combination of explicit (and implicit) mixing in the Eulerian model removes much of this variability but yields better agreement with the measurements overall. We therefore explore a simple treatment of mixing in the Lagrangian model that, drawing on output from the Eulerian model, offers a compromise between the two models. We use this Lagrangian/Eulerian combination, in addition to the separate Eulerian and Lagrangian models, to simulate ozone at a site in the boundary layer downwind of Manaus, Brazil. The Lagrangian/Eulerian combination predicts a value for an AOT40-like accumulated exposure metric of around 1000 ppbv h, compared to just 20 ppbv h with the Eulerian model. The model framework therefore has considerable bearing on our understand-

ing of the frequency at which, and the duration for which, the rainforest is exposed to damaging ground-level ozone concentrations.

1 Introduction

Though not all plants emit isoprene, around 500 Tg(C) isoprene are emitted from vegetation globally each year (Guenther et al., 2006; Arneth et al., 2008). This exceeds the annual carbon flux attributable to anthropogenic non-methane volatile organic compounds (NMVOCs) by a factor of ten; see, e.g., WMO (1995). Isoprene is also highly reactive, with a lifetime of the order of minutes with respect to oxidation by the hydroxyl radical (OH), compared to around 10 years in the case of methane (CH_4). Biogenic isoprene emissions thus have the potential to profoundly affect tropospheric OH. Moreover, since OH is the main chemical species responsible for removing gaseous pollutants, including some potent greenhouse gases (e.g. CH_4), isoprene emissions have a bearing on both air quality and climate. These influences are furthered through the impact that isoprene emissions have on tropospheric ozone (O_3), which is both a respiratory aggravant and a greenhouse gas (see, respectively, WHO, 2000; IPCC, 2002). High O_3 concentrations at ground level also cause visible leaf-injury to plants, reducing the rates at which they photosynthesise and increasing their requirements of resources to detoxify and repair (e.g. Ainsworth et al., 2012); their detrimental impact on crop yields, for example, is well documented (e.g. Avnery et al., 2011). There is thus a feedback between the health of the Amazon rainforest and the composition of air above it, with potentially significant implications for the tropical carbon cycle (Sitch et al., 2007; Pacifico et al., 2015); it is interesting that the chemistry in the pristine rainforest environment ("NO_x limited"; see later) tends to yield low O_3 concentrations – in favour of the forest's health. However, despite these important effects, our ability to capture the influence of isoprene emissions on tropospheric OH and O_3 has been in question since Lelieveld et al. (2008) and Butler et al. (2008) reported observations of unexpectedly high OH concentrations in the boundary layer over the Amazon basin

– a very strong source of isoprene – that could not be reproduced with then-current atmospheric chemistry models. The incompatibility of measured and modelled OH and isoprene was further demonstrated for the Borneo rainforest by Pugh et al. (2010, 2011) and Stone et al. (2011). Whilst heterogeneous chemistry is not considered in this study, isoprene also interacts with air pollution and the climate system by acting as a precursor to secondary biogenic organic aerosol, with an aerosol yield of a few percent (e.g. Carlton et al., 2009; Chen et al., 2015).

The specific difficulty Lelieveld et al. (2008) and Butler et al. (2008) faced was explaining observations of simultaneously high isoprene- and OH concentrations, made during the Guyanas Atmosphere–Biosphere exchange and Radicals Intensive Experiment with a Learjet campaign of 2005 (GABRIEL; see Atmospheric Chemistry and Physics Special Issue 88). High isoprene emissions were expected to sustain high isoprene concentrations whilst suppressing OH concentrations (due to the rapid reaction between the two). It was the unexpectedly high OH concentrations that led Lelieveld et al. (2008) to speculate that the chemistry models were missing a mechanism by which some of the OH initially consumed in isoprene oxidation was "recycled". Meanwhile, Butler et al. (2008) explored the role that the physical separation, or "segregation", of air masses containing isoprene emissions could play in resolving the apparent paradox, as have Pugh et al. (2011) since; see later. Here, we confront two atmospheric chemistry models, and modelling frameworks (Eulerian and Lagrangian), with recent airborne measurements of atmospheric composition above the Amazon rainforest, made during the South AMerican Biomass Burning Analysis campaign of 2012 (SAMBBA; see Darbyshire and Johnson, 2013). Building on the recent studies of Squire et al. (2014, 2015), we compare the abilities of these models subject to two chemical mechanisms – one including an OH "recycling" mechanism that should prove effective in pristine Amazon environments. In the Lagrangian model, motivated by studies such as Kuhn et al. (2010), we also explore the impact that the spatial resolution of trace gas emissions has on our ability to capture the atmospheric chemistry, and

Isoprene chemistry in pristine and polluted Amazon environments

J. G. Levine et al.

Title Page

Abstract	Introduction
Conclusions	References
Tables	Figures

|◄ | ►|

◄ | ►

Back | Close

Full Screen / Esc

Printer-friendly Version

Interactive Discussion

hence the impact of ground-level O_3 on the health of the rainforest, in polluted plumes downwind of the city of Manaus.

Squire et al. (2014) explored the impacts that possible future changes in isoprene emissions – stemming from changes in atmospheric CO_2, the physical climate (e.g. surface air temperatures), and anthropogenic land use – could have on tropospheric O_3. They did so using a global Eulerian chemistry-climate model, the UK Met Office Unified Model (UM; Hewitt et al., 2011) coupled to the UK Chemistry and Aerosol model (UKCA; O'Connor et al., 2014), jointly referred to as UM-UKCA. We use the same Eulerian model here, building on much of Squire et al. (2014, 2015)'s work as outlined in the next section. Squire et al. (2014) employed isoprene emissions calculated using parameterisations based on the Model of Emissions of Gases and Aerosols from Nature (MEGAN; Guenther et al., 2006), with vegetation simulated offline using the Sheffield Dynamic Global Vegetation Model (SDGVM; Beerling et al., 1997; Beerling and Woodward, 2001) as described by Lathière et al. (2010). Before exploring the impact of changes in isoprene emissions, Squire et al. (2014) demonstrated that UM-UKCA showed some skill at reproducing recent observations of tropospheric O_3 when employing present day emissions: they compared their simulated profiles of O_3 with sonde profiles from the Southern Hemisphere ADditional OZonesondes network (SHADOZ; Thompson et al., 2003). Notably, however, this network did not offer measurements of tropospheric O_3 above the Amazon rainforest – globally, responsible for almost half of all biogenic NMVOC emissions (Guenther et al., 1995) and the greatest source of isoprene (see, e.g., Fig. 2 of Squire et al., 2014). Squire et al. (2015) then explored the sensitivity their projections of future tropospheric O_3 showed to the chemical mechanism they employed. However, they did not explore the impact of this mechanism on their ability to reproduce present day observations.

Here, we test the ability of (i) a nudged version of UM-UKCA and (ii) a Lagrangian model, the Cambridge Tropospheric Trajectory model of Chemistry And Transport (CiT-TyCAT; Pugh et al., 2012), to simulate SAMBBA measurements above the Amazon. In each model, we carry out (otherwise identical) integrations employing two of the four

chemical mechanisms explored by Squire et al. (2015): the UM-UKCA Chemistry of the Troposphere (CheT), in which isoprene oxidation follows the Mainz Isoprene Mechanism (MIM; Pöschl et al., 2000); and an updated version of this mechanism (CheT2) that incorporates the recent developments in our understanding of this chemistry compiled for the UK Met Office by Jenkin (2012). CheT, being based on the MIM, contains similar chemistry to the models with which Lelieveld et al. (2008) and Butler et al. (2008) were unable to simulate the simultaneously high isoprene- and OH concentrations observed during the GABRIEL campaign. Meanwhile, the updates in CheT2 include an efficient route by which OH initially consumed in isoprene oxidation may be regenerated at low ambient concentrations of nitrogen oxides ($NO_x = NO + NO_2$): the formation of hydroperoxy-aldehydes from hydroperoxy radicals and their subsequent rapid release of OH (Peeters et al., 2009; Crounse et al., 2011).

Questions remain regarding the effect that the "segregation" of air masses containing isoprene emissions has on the chemistry ensuing therein. In large-eddy simulations of a convective boundary layer, Krol et al. (2000) found that it could reduce the effective rate of reaction between OH and a generalised hydrocarbon by as much as 30 %, relative to that simulated in a box model. They obtained the largest reductions when the hydrocarbon was emitted non-uniformly and assumed to react rapidly with OH. Recall that the emissions of isoprene are not expected to be uniform, since not all plants emit isoprene, and isoprene is highly reactive towards OH. It was in this context that Butler et al. (2008) explored the role that segregation could play in reconciling the simultaneously high isoprene- and OH concentrations observed during the GABRIEL campaign. They found that a 50 % reduction in the "effective rate constant" for this reaction was required, implying a high degree of segregation. Though Butler et al. (2008) recognised that the measurements were not of sufficient spatial- and temporal resolution to confirm such segregation, they believed that the high degree of variability observed in isoprene concentrations rendered this not implausible. Pugh et al. (2010) subsequently explored a 50 % reduction in the rate of this reaction, in an effort to reconcile measurements from the Oxidant and Particle Photochemical Pro-

cesses campaign above a South-East Asian tropical rainforest campaign (OP3; Hewitt et al., 2010) with simulations using CiTTyCAT. Later, explicitly exploring segregation using observed variability in isoprene, Pugh et al. (2011) found that segregation alone could not fully account for the difference between modelled and measured OH. CiTTy-CAT is ill-suited to exploring the effects of segregation in a convective boundary layer, since the transport of each air parcel is described by a trajectory that at best captures regional-to continental scale convection (see next section). However, it does allow us to simulate, independently, the chemistry taking place in air parcels arriving at points spaced only a short time apart on a flight track, in other words assuming no mixing occurs between them; we have the option of then adding a simple treatment of mixing such as relaxation towards background composition. More sophisticated treatments of mixing between ensembles of trajectories are possible using a variant of the CiTTyCAT model (see Pugh et al., 2012; Cain et al., 2012), but we begin here by focussing on the simulation of independent air parcels. This makes for an interesting comparison with simulations using UM-UKCA, which implicitly mixes air on the scale of the model grid ($3.75° \times 2.5°$ in "climate mode"). CiTTyCAT should yield greater variability in simulated isoprene concentrations: Lagrangian box models, run in "domain-filling" mode, capture much of the strain-induced stirring of the atmosphere, with no mixing, whilst Eulerian models capture the large-scale stirring but inevitably introduce mixing as they average concentrations across grid boxes (see, e.g., Dragani et al., 2002; Methven et al., 2003).

The mixing of air within the models, or lack thereof, has further effects on the chemistry simulated. Most pertinent to this study is the effect of mixing on the concentration of NO_x, specifically the NO_x : VOC ($CH_4 + NMVOCs$) ratio; see, for example, the results of the Empirical Kinetics Modelling Approach of Dodge (1977) and Sillman and He (2002). At very low NO_x : VOC ratios, we expect isoprene to remove O_3 (through direct reaction with it); at moderate-to-high NO_x : VOC ratios, OH-initiated isoprene oxidation should produce O_3 with increasing efficiency as the NO_x : VOC ratio increases; until, at very high NO_x : VOC ratios encountered only in the most polluted urban and industrial environments, this O_3 production is partially offset by O_3 titration. The effects, therefore,

that NO$_x$ emissions from a city like Manaus (in the middle of the Amazon rainforest) have on the concentration of O$_3$ simulated downwind could strongly depend on the mixing, or "smearing out", of NO$_x$ emissions. Crudely, we can caricature the chemistry over the Amazon as being fuelled by isoprene emissions, with the consequences of that chemistry for tropospheric O$_3$ being determined by the ambient NO$_x$: VOC ratio. The smearing out of NO$_x$ emissions could conceivably "flip" the result of this chemistry from predominantly net O$_3$ destruction, with isolated pockets of intense net O$_3$ production, to less intense net O$_3$ production, pervasive over a much larger area. The knock-on effects of these contrasting results for the health of the rainforest – exposed to different concentrations of O$_3$, and different degrees of O$_3$ variability – could differ markedly. It is in this context that we take the opportunity, in the Lagrangian model, to explore the impact of emission resolution on our simulation of atmospheric chemistry and composition at low altitudes downwind of Manaus: we carry out otherwise identical integrations employing anthropogenic emissions from Version 4.2 of the Emissions Database for Global Atmospheric Research (EDGAR; European Commission, 2009) at their full 0.1° × 0.1° resolution and degraded to the 3.75° × 2.5° grid used in UM-UKCA (in "climate mode").

In the next section, we describe: the SAMBBA measurements with which we compare model simulations (Sect. 2.1); the Eulerian and Lagrangian models we use, UM-UKCA and CiTTyCAT (Sect. 2.2); the two chemical mechanisms we explore, CheT and CheT2 (Sect. 2.3), and the trace gas emissions we employ (Sect. 2.4). We present the results in Sect. 3 and discuss them with reference to the literature in Sect. 4.

2 Method

2.1 SAMBBA measurements

The SAMBBA campaign aimed to study the impact of biomass burning on atmospheric composition and climate over the Amazon basin. To this end, a total of 20 flights were

flown with the UK's Facility for Airborne Atmospheric Measurements' (FAAM) BAe-146 in September and October 2012 (the dry season and "biomass burning season"). We focus, however, on five flights aimed at characterising the "background" composition of the atmosphere in that region – the influence of biogenic emissions in the absence of biomass burning: B735, B744, B745, B749 and B750. Some portions of these flights still intercepted air influenced by biomass burning upwind, but considerably less than those flights specifically aiming to probe this influence. Chemically, we focus on measured concentrations of five species central to gas-phase tropospheric chemistry: O_3, NO, NO_2, isoprene (C_5H_8) and carbon monoxide (CO). We have no measurements of OH concentration with which to compare our simulated OH concentrations. However, the comparison of measured and modelled O_3 concentrations is nonetheless valuable in the context of isoprene oxidation and its impact on OH, since: OH is derived from O_3 (by O_3 photolysis and reaction of the resulting excited $O(^1D)$ oxygen atoms with water vapour); and, if a model were to reproduce measurements of OH concentration but not O_3 concentration, it would be simulating OH well but for the wrong reason(s).

2.1.1 SAMBBA flight tracks (and the histories of air parcels encountered)

The thick black lines in Fig. 1 illustrate the flight tracks in longitude and latitude of flights B735, B744, B745, B749 and B750. (The variation in altitude during each flight is illustrated in subsequent figures comparing measured and modelled trace gas concentrations.) Superimposed on each of these panels in Fig. 1, are 7 day back-trajectories describing the calculated routes by which the air sampled at points spaced one minute apart along each flight track reached those locations; the bottom right panel illustrates the 7 day back-trajectories calculated from the (arbitrary) site we explore downwind of Manaus; the "×" marks the site (61.0° W, 3.1° S) and the dot marks Manaus. The trajectories are coloured according to their pressures, providing some indication of where air parcels might have picked up emissions (e.g. at pressures greater than 800–900 hPa, corresponding to altitudes of less than roughly 1–2 km). The trajectory calculations are described later (Sect. 2.2.2) but, for the time being, we note two points: the divergence

of air parcels backwards in time (i.e. with increasing distance from the fight tracks), which offers the Lagrangian model an opportunity to capture diversity in initial composition that may be lost or less well resolved in the Eulerian model; and the general consistency of colour along any one trajectory bound for a flight track, indicating that many air parcels have spent much of the 7 days prior to arrival on the flight track at approximately the same pressure. This implies that air parcels encountered in low-altitude portions of the flights have often spent much of the last 7 days at low altitudes and, thus, exposed to trace gas emissions (and dry deposition) in the boundary layer; air parcels encountered in high-altitude portions of the flights, on the other hand, have often spent much of the last 7 days well above the boundary layer and hence exempt from these influences. The trajectories bound for the site downwind of Manaus, meanwhile, appear to descend over the course of 7 days from origins in the mid troposphere to the site in the boundary layer (900 hPa) and are thereby predominantly exposed to trace gas emissions (and dry deposition) in the latter half of their journeys.

2.1.2 O_3 measurements

O_3 was measured at 0.1 Hz by a Thermo Environmental UV absorption photometer model 49C, traceable to the UK National Physical Laboratory primary ozone standard with an uncertainty of 2 %, and a precision of 1 ppb.

2.1.3 NO and NO_2 measurements

NO_x was measured from the aircraft using a high sensitivity NO_x chemiluminescence system built by Air Quality Design, Inc. The instrument has a dual channel architecture for independent quantification of NO and NO_2, with each channel having a sample flow of 1 L min^{-1}. NO is measured in one channel by an established chemiluminescence technique (Lee et al., 2009), with NO_2 quantified in a second channel by photolytic conversion to NO using blue light emitting diodes centred at 395 nm. The 395 nm wavelength has a specific affinity for NO_2 photolytic conversion to NO, giving high analyte

selectivity within the channel. Work by Pollack et al. (2010) evaluated the relative high NO_2 affinity for conversion of NO_2 to NO using 395 nm blue light LEDs. They highlighted the low probability of other species within the gaseous chemical matrices such as nitrous acid (HONO), being affected by the 395 nm light, so in turn reducing possible non NO_2 species interfering with the measurement. NO_x was then quantified by ozonation of the subsequent total NO present in the reaction vessel after conversion with NO_2 derived from the difference between NO_x and NO mixing ratios.

The instrument was calibrated by adding a small flow (5 sccm) of known NO concentration (5 ppmv – Air Liquide) into the ambient sample flow, resulting in around 10 ppbv of NO. The conversion efficiency of the NO_2 converter was measured during each calibration by gas phase titration of the NO to NO_2 by addition of O_3. In flight calibrations were always carried out above the boundary layer, thus ensuring low and stable background levels of NO_x. Typically calibrations are carried out at the beginning and end of a flight, with sensitivities and conversion efficiency interpolated between the two and applied to all data. Detection limits for the 10 s averaged data were ~ 10 pptv for NO and 15 pptv for NO_2 with approximate total errors at 1 ppbv being 10 and 15 % for NO and NO_2 respectively.

2.1.4   CO measurements

CO was measured at 1 Hz by an Aerolaser VUV fluorescence analyser model AL5002 (Gerbig et al., 1999). The instrument was calibrated in-flight using an air standard, traceable to the World Meteorological Organisation CO scale X2004, with a 2 % uncertainty, and 3 ppb precision.

2.1.5 C_5H_8 measurements

Isoprene was measured using an on-board proton transfer reaction mass spectrometer containing a quadrupole detector (PTR-MS, Ionicon Analytik GmbH, Innsbruck, Austria). During the SAMBBA campaign, the instrument measured a range of hydrocar-

bons and oxygenated hydrocarbons with a typical cycle time of 3–5 s. Isoprene mixing ratios were determined using a dynamically-diluted calibrated gas standard (~ 500 ppb in nitrogen, uncertainty ±5 %, Apel-Reimer, Boulder CO). For the purposes of this comparison we have applied a 15-point smoothing function to the high frequency data to give an approximately 1 min moving averaged mixing ratio. The mean limit of detection for isoprene under these conditions was 110 ppt. The overall measurement uncertainty is estimated to be ±15 %. Full instrumental, operational and calibration details are described in Murphy et al. (2010).

Additionally, whole air samples (WAS) were collected on flights B735 and B749, and subsequently analysed to measure isoprene mixing ratios. The WAS system, described in greater detail by Lidster et al. (2014), comprises sixty four canisters with fused silica deactivated inner surfaces, each with three litre internal volume. Individual canisters were filled at operator-determined times using a double-headed metal bellows pump (all stainless steel components) to a final pressure of up to 40 psi and shipped back to the UK for analysis within one month of collection. Analysis was performed using a dual channel gas chromatograph with flame ionisation detectors, described in detail by Hopkins et al. (2011), which was calibrated using a certified standard supplied by the National Physical Laboratory (Ozone precursors mix, cylinder number D641613). Detection limits were in the single parts per trillion range with typical calculated uncertainties of between 3 and 20 %.

2.2 UM-UKCA and CiTTyCAT models

2.2.1 UM-UKCA (Eulerian model)

We start from the setup of UM-UKCA, employing present day boundary conditions, that Squire et al. (2014) demonstrated had some skill at reproducing recent tropospheric O_3 observations (sonde profiles from the SHADOZ network; see their Fig. 3). This setup, similar to that described by Telford et al. (2010), was comprised of the Hadley Centre Global Environment Model version 3 – Atmosphere only (HadGEM3-A r2.0) at

UM version 7.3 (Hewitt et al., 2011) and UKCA TropChem (O'Connor et al., 2014). For full details, the reader is referred to Squire et al. (2014). Here, we simply note that the model was run in "climate mode" – at a relatively low spatial resolution, N48 L60 (3.75° longitude × 2.5° latitude; 60 hybrid height levels stretching from the surface to around 84 km) – and employed the standard tropospheric chemistry mechanism, CheT. This is the setup that Squire et al. (2015) subsequently used in their "BASE CheT" experiment. Their "BASE CheT2" experimental setup was identical except for employing the updated CheT2 chemistry. Here, we carry out two integrations with UM-UKCA based on Squire et al. (2015)'s BASE CheT and BASE CheT2 experiments: UM-UKCA (CheT) and UM-UKCA (CheT2), respectively.

Our integrations differ from Squire et al. (2015)'s in four ways: we employ different trace gas emissions, as outlined in Sect. 2.4; we nudge UM-UKCA towards European Centre for Medium-range Weather Forecasts (ECMWF) ERA Interim analyses, as described by Telford et al. (2009); we run the model for just less than 9.5 months (8 months from 00:00 UT 2 January 2012 to spin the model up from BASE CheT and BASE CheT2 start dumps, and a further 40 days from 00:00 UT 2 September 2012 to cover the SAMBBA campaign period); and we output the concentrations of all chemical species at points spaced one minute apart along each of the five SAMBBA flights, using Telford et al. (2013)'s flight track code. Note that we also output the concentrations of all chemical species simulated at the times and locations of the air parcel trajectories 7 days previously, based on the back-trajectory calculations mentioned in Sect. 2.1.1. These data are used to initialise the integrations with CiTTyCAT. Likewise, when modelling the composition of air downwind of Manaus, we provide UM-UKCA with an artificial "flight track" to output the concentrations of chemical species simulated at 6 hourly intervals (throughout September 2012) at a boundary layer site (61.0° W, 3.1° S, 900 hPa) roughly 100 km downwind (1° west) of Manaus, and at the locations of the corresponding air parcels 7 days previously – based on further back-trajectory calculations.

2.2.2 CiTTyCAT (Lagrangian model)

CiTTyCAT r4.2.1 (Pugh et al., 2012) is a Lagrangian model of atmospheric chemistry and transport, stemming from the Cambridge Tropospheric Trajectory model of Chemistry And Transport (Wild et al., 1996). This is not the first time that CiTTyCAT has been used to simulate atmospheric chemistry and composition over a tropical rainforest: Pugh et al. (2010), as briefly referred to in the introduction, tested the performance of the model in two-box mode (two boxes, to account for the nocturnal collapse of the boundary layer and development of a residual layer above it), confronting it with measurements made during the OP3 campaign at Danum Valley, Malaysian Borneo. We use the model in single trajectory mode (moving a single model box along one trajectory at a time) many times over as we loop over all back-trajectories bound for (a) the arrival points spaced one minute apart on the five SAMBBA flights, and (b) the receptor site downwind of Manaus at 6 hourly intervals throughout September 2012. The single trajectory mode has been used extensively in previous studies of long range transport (see, e.g., Wild et al., 1996; Evans et al., 2000; Real et al., 2007, 2008). Note that the treatment of transport constitutes the main difference between CiTTyCAT and UM-UKCA: transport in the Lagrangian framework is described by discrete trajectories (series of times and locations) calculated offline, as opposed to fluxes between adjacent model boxes in a fixed 3-D Eulerian grid.

The back-trajectories, illustrated in Fig. 1, are calculated using ROTRAJ (Methven, 1997) in conjunction with ECMWF ERA Interim analyses, as previously outlined by Pugh et al. (2012). The analysed wind fields, available at 6 hourly intervals (00:00 UT, 06:00 UT, 12:00 UT and 18:00 UT) are interpolated linearly in space and time. The location of each trajectory is then calculated by integrating the interpolated wind velocities with respect to time according to the fourth order Runge–Kutta method (Methven, 1997) and recorded every 6 h together with the air temperature and specific humidity, which are also interpolated in space and time from the analyses.

Title Page

Abstract | Introduction

Conclusions | References

Tables | Figures

|◄ | ►|

◄ | ►

Back | Close

Full Screen / Esc

Printer-friendly Version

Interactive Discussion

To ensure the transport in the two models is broadly consistent, we use the same analyses to calculate the trajectories as we use to nudge UM-UKCA (see above). However, two key differences remain. Firstly, the trajectory calculations exploit the full-resolution of the analysed winds (roughly $0.7° × 0.7°$) whilst UM-UKCA is nudged towards these winds following degradation to the resolution of its Eulerian grid ($3.75° × 2.5°$ in "climate mode"). The transport in CiTTyCAT is therefore more finely resolved and should yield greater structure in the composition of air it simulates along each flight track, and downwind of Manaus, particularly when combined with high resolution trace gas emissions. The transport in CiTTyCAT, however, only includes convection as captured by the analyses (i.e. large-scale convection) whilst UM-UKCA explicitly adds updrafts and downdrafts associated with convection on smaller scales, following Gregory and Rowntree (1990) and Gregory and Allen (1991). CiTTyCAT therefore lacks a certain amount of vertical mixing. Some mixing within the boundary layer is included implicitly, as the addition of emissions (conversion from mass fluxes to enhancements in concentration) depends on a length scale associated with the height of the boundary layer, but no ventilation of the boundary layer or exchange with the free troposphere is included. We focus first on the simulation of independent air parcels – with no vertical (or horizontal) mixing – to explore the influence of contrasting air parcel histories on the chemistry ensuing therein. However, we subsequently explore the sensitivity of some of our results to a simple treatment of diffusive vertical mixing.

The treatment of diffusive vertical mixing, described by Pugh et al. (2012), comprises relaxation towards background composition at rates specified by free-troposphere and boundary-layer diffusion coefficients, κ_{FT} and κ_{BL}. These yield relaxation timescales of $\tau_{FT} = D^2/(2\kappa_{FT})$ and $\tau_{BL} = BLH^2/(2\kappa_{BL})$, where D is a free tropospheric depth parameter and BLH is boundary layer height. Pugh et al. (2012) suggest κ_{FT} should typically take values of between $0.5\,m^2\,s^{-1}$ (under stable conditions) and $1.5\,m^2\,s^{-1}$ (under more turbulent ones); Pisso et al. (2009) reported slightly lower values of $0.3–1.0\,m^2\,s^{-1}$. Typically, $\kappa_{BL} = 10\kappa_{FT}$ whilst D takes values of roughly 200–500 m. We explore the impact of mixing subject to three different combinations of κ_{FT}, κ_{BL} and D (Mix1, Mix2 and

Mix3) that span the ranges suggested by Pugh et al. (2012); these are given in Table 1 together with the τ_{FT} and τ_{BL} they yield. For species of intermediate lifetime (O_3, CO, C_2H_6, C_3H_8 and PAN), we relax the concentrations simulated in CiTTyCAT towards 3-D monthly mean (September 2012) concentrations calculated in the UM-UKCA in-
5 tegration employing the same chemical mechanism; the five SAMBBA flights, and the back-trajectories calculated from those, fall within September 2012, as do the bulk of the back-trajectories bound for the site downwind of Manaus during this month. We relax the concentrations of all short-lived species towards zero concentrations (charac-teristic of the free troposphere), whilst that of CH_4 is fixed at 1.76 ppmv.

10 The integrations with CiTTyCAT are carried out subject to eight model setups; these are summarised in Table 2. We simulate the measurements made on the five SAMBBA flights (B735, B744, B745, B749 and B750) subject to setups 1–4, exploring the impact of different chemical mechanisms (CheT and CheT2; described in more detail in the next section) and different resolutions of trace gas emissions ("UKCA res" and "High
15 res"; described in Sect. 2.4). With setups 5 and 6, we then explore the sensitivity of our simulations of flight B735 to the inclusion of diffusive vertical mixing as described above. We do so in order to assess to what extent differences between simulations with CiTTyCAT and UM-UKCA can be thus reduced; setups 5 and 6 therefore employ UKCA res emissions. Finally, we model the composition of the atmosphere downwind of Man-
20 aus throughout September 2012 subject to setups 3–8. Our aim here is to capture the episodic influence of anthropogenic emissions from Manaus, and we therefore chiefly adopt setups employing High res emissions (3, 4, 7 and 8). We continue, however, to explore the sensitivity of our results to emission resolution, hence including setups 5 and 6, in addition to both the choice of chemical mechanism and the inclusion/exclusion
25 of vertical mixing.

To reduce the differences between the two models, aside from those intrinsic to their different frameworks, we ensure that precisely the same chemical mechanisms and chemical reaction rate coefficients are used in CiTTyCAT as in UM-UKCA (Squire et al., 2014, 2015). Likewise, we employ the same dry deposition velocities and Henry

coefficients in the two models (Squire et al., 2014, 2015), and we use 3-D fields of precipitation, output from UM-UKCA every 20 min timestep, to drive the wet deposition in CiTTyCAT. This is in addition to initialising the composition of air parcels in CiTTy-CAT with the concentrations of species simulated in UM-UKCA (subject to the same

5   chemical mechanism) as described at the end of the last section.

2.3   CheT and CheT2 chemical mechanisms

The standard tropospheric chemistry mechanism, CheT, includes 56 chemical tracers and 165 photochemical reactions, of which 16 tracers and 44 reactions comprise the MIM (Pöschl et al., 2000). It is the result of a systematic reduction of version 2 of the

10 Master Chemical Mechanism (MCM; Jenkin et al., 1997), in which species are lumped together based on their structure, for example all hydroxyperoxy radicals as "ISO_2". CheT2 differs only with respect to isoprene oxidation, with 24 tracers and 59 reactions in place of the previous 16 and 44 respectively, and is traceable to MCM version 3.2 (MCMv3.2). The differences, reflecting the updates compiled by Jenkin (2012) for the

15 UK Met Office, are as follows:

1. Changes to the chemistry of first generation isoprene nitrates (ISON): NO_x is regenerated from ISON in CheT by photolysis, or conversion to second gener-ation nitrates (NALD), followed by reaction with OH; in CheT2, the yield of NO_x from ISON is increased in line with the measurements of Perring et al. (2009)

20   by increasing the rate of ISON photolysis and adding a further $ISON + OH \rightarrow NO_2$ channel; CheT2 also includes the addition of O_3-initiated ISON degradation (Lock-wood et al., 2010).

2. The inclusion, as mentioned in Sect. 1, of a route by which OH initially consumed in isoprene oxidation may be efficiently regenerated at low ambient NO_x con-

25   centrations: the formation of hydroperoxy-aldehydes (HPALDS) from hydroperoxy radicals (ISO_2) and their subsequent rapid release of OH (Peeters et al., 2009; Crounse et al., 2011).

Title Page

Abstract   Introduction

Conclusions   References

Tables   Figures

◀   ▶|

◀   ▶

Back   Close

Full Screen / Esc

Printer-friendly Version

Interactive Discussion

3. The inclusion of the formation of isoprene epoxydiols (IEPOX) from the oxidation of isoprene hydroxyl-hydroperoxides (ISOOH); Paulot et al. (2009) identified these as a potential source of secondary organic aerosols.

4. A reduction in the yield of peroxymethacrylic nitric anhydride (MPAN) from isoprene oxidation relative to that adopted in CheT; see Jenkin (2012) for details.

In this study, however, we are less concerned with the differences between the two mechanisms, which have already been explored at length (see, e.g., Archibald et al., 2010a, b; Squire et al., 2015), than we are with their relative abilities to reproduce observations of atmospheric composition above the Amazon rainforest – and the latter subject to different model frameworks (Eulerian and Lagrangian) and trace-gas emissions.

2.4 Trace gas emissions

The trace gas emissions are comprised of: anthropogenic emissions taken from EDGAR version 4.2 (http://edgar.jrc.ec.europa.eu); and biogenic emissions calculated with the Organising Carbon and Hydrology In Dynamic Ecosystems land surface model (ORCHIDEE), with the exception of NO_2 emissions from soils that are taken from the Global Emissions Inventory Activity (GEIA; Yienger and Levy, 1995). The annual total emission of each species, globally, is given in Table 3, including its breakdown into anthropogenic and biogenic components.

We employ EDGAR 4.2 emissions of NO_2, CO and NMVOCs from all sectors apart from "Non-road transportation" (1A3a + c + d + e in the nomenclature of the Intergovernmental Panel on Climate Change; IPCC), since the latter includes aircraft emissions that are difficult to implement in the Lagrangian model; CH_4 is treated as a constant field (1.76 ppmv). We adopt the most recent emissions available, which correspond to the year 2008. Available at a spatial resolution of up to $0.1° × 0.1°$ globally, these are capable of resolving a city of approximately 10 km × 10 km in the tropics, such as Manaus. We note, however, that they do not include any seasonality; we expect the

seasonality to be relatively low in the tropics. The NMVOC emissions come lumped together as a single carbon flux. We derive emissions of ethane (C_2H_6), propane (C_3H_8), formaldehyde (HCHO), acetone ($CH_3C(O)CH_3$) and acetaldehyde (CH_3CHO) from this using the IPCC (2002)'s speciation of industrial- and biomass burning emissions; see their Table 4.7(b). This speciation is crude: we assume, for example, that "ketones" are entirely comprised of $CH_3C(O)CH_3$, and "other aldehydes" solely CH_3CHO. However, our priority is to start from anthropogenic emissions of sufficient spatial resolution to resolve the city of Manaus, and EDGAR 4.2 is unique in providing emissions of this resolution, globally. The CiTTyCAT integrations employing "High res" emissions exploit their full $0.1° \times 0.1°$ resolution. For use in UM-UKCA, and the CiTTyCAT integrations employing "UKCA res" emissions, the emissions are degraded to $3.75° \times 2.5°$; see Table 2 and accompanying text.

As stated above, biogenic emissions of C_5H_8, HCHO, $CH_3C(O)CH_3$ and CH_3CHO are calculated with ORCHIDEE. This includes parameterisations based on Guenther et al. (1995) and Lathière et al. (2006), modified according to Guenther et al. (2012) and more recent findings to take into account the progress of our knowledge in this field (see Messina et al., 2015). ORCHIDEE is forced with 2012 National Centers for Environmental Prediction meteorological analyses (NCEP v5.3) from the Climatic Research Unit of the US National Centre for Atmospheric Research. These daily (24 h average) emissions are used at full spatial resolution ($0.5° \times 0.5°$) in the "High res" integrations with CiTTyCAT but, just as for the anthropogenic emissions, degraded to $3.75° \times 2.5°$ for use in UM-UKCA and the CiTTyCAT integrations employing "UKCA res" emissions. We apply a diurnal cycle – the same in both models, based on the division of each 24 h period into 20 min intervals – to the emissions of C_5H_8 but not HCHO, $CH_3C(O)CH_3$ or CH_3CHO. The NO_2 emissions from soils are taken from GEIA dataset, soilNOXmn1.1a (Yienger and Levy, 1995). In view of the uncertainty in these, they are used in both models, in all integrations, at a resolution of $3.75° \times 2.5°$.

Figure 2 illustrates the total "UKCA res" emissions of each species (anthropogenic + biogenic) on the 1 January and 1 July 2012. Recall, only the species including a bio-

genic component show seasonality. Meanwhile, Fig. 3 compares the monthly mean total "UKCA res" and "High res" emissions of each species encountered in September 2012, over the same domain as the flight tracks and back-trajectories are illustrated in Fig. 1; note that the influence of the low resolution NO_2 emissions from soils are still

5 visible in the "High res" NO_2 emissions here.

3 Results

3.1 Comparing Eulerian and Lagrangian model frameworks

We start by comparing the measurements of O_3 on flight B735 (from Porto Velho, just south of the State of Amazonas, north east to Manaus; see Fig. 1) with those simulated

10 in UM-UKCA (CheT) and CiTTyCAT (CheT); see Fig. 4. We do not quantify the skill that each model shows with regards to reproducing the measurements; we focus instead on the qualitative nature of the model simulations and how the simulations differ from each other. We examine modelled and measured [NO], [NO_2], [C_5H_8] and [CO] below. The corresponding figures for flights B744, B745, B749 and B750 are included as

15 Supplement; any differences in findings are noted in the text that follows. UM-UKCA (CheT) and CiTTyCAT (CheT) employ the same chemical mechanism (CheT) and the same trace gas emissions (UKCA res). We can thus compare these experiments, one carried out in an Eulerian framework (UM-UKCA; solid blue line), the other in a Lagrangian framework (CiTTyCAT; solid green line) following initialisation with data from

20 UM-UKCA (dashed blue line). We do so in the context of the SAMBBA measurements (grey line); the red line (not included in the legend) illustrates the altitude of the aircraft on this flight.

In the middle troposphere (2500–7500 m), both models tend to overestimate measured [O_3], but particularly CiTTyCAT. At these altitudes, the [O_3] simulated in CiTTy-

25 CAT strongly depends on that with which it is initialised 7 days previously (based on output from UM-UKCA): the green line closely follows the dashed blue line in these por-

tions of the flight (around 12.5, 13.5, 14.5 and 15.5 UT; 08:30, 09:30, 10:30 and 11:30 LT). This is consistent with the air parcels during those periods generally not encountering the boundary layer (altitudes of less than 1000–2000 m) during the previous 7 days; see Fig. 1 and accompanying text. Since these air parcels are subject to neither emissions nor dry deposition, the small differences between the green and dashed-blue lines are due to intervening chemistry and/or wet deposition. The $[O_3]$ simulated with CiTTyCAT also shows much more structure in these regions than that simulated with UM-UKCA. The initialisation is responsible for this additional structure – the result of divergent air parcel histories (see Sect. 2.1.1 and, again, Fig. 1) – note that it is largely retained in CiTTyCAT over the course of 7 days but almost entirely lost in UM-UKCA. Compared to the measurements, CiTTyCAT shows too much structure (perhaps due to the lack of explicit mixing in the model) whist UM-UKCA shows too little (presumably due to mixing on the scale of its $3.75° \times 2.5°$ grid); see discussion in Sect. 2.2.2 of the differences in transport, especially mixing, between the two models. A combination of the two models, such as the simple treatment of diffusive vertical mixing described earlier (relaxation of CiTTyCAT towards UM-UKCA), would likely yield best agreement with the measurements in this respect; see later. We note, however, that on two flights in which the measurements of $[O_3]$ at high altitudes show less structure (B744 and B749), UM-UKCA yields much better agreement with the measurements; see Figs. S1 and S3 in the Supplement.

At low altitudes (0–1500 m), UM-UKCA tends to overestimate measured $[O_3]$ whilst CiTTyCAT generally shows good agreement; the exception is the period shortly after 13:00 UT in which UM-UKCA shows good agreement and CiTTyCAT underestimates the measurements. Generally, CiTTyCAT simulates lower $[O_3]$ than UM-UKCA in these low altitude regions and yields better agreement with measured $[O_3]$ here. Similar behaviour is observed on flights B749 and B750 (see Figs. S3 and S4). We note, however, that this does not extend to all low-altitude portions of flights B744 and B745 (see Figs. S1 and S2); on these two flights, at altitudes towards the top end of the 0–1500 m range, possibly bordering on the free troposphere, CiTTyCAT starts to yield

higher [O_3] than UM-UKCA as it did at mid-to-high altitudes. But, continuing to examine flight B735, what is interesting is that the [O_3] simulated in CiTTyCAT at low altitudes differs markedly from that with which it is initialised, consistent with this being strongly influenced by intervening emissions, chemistry and/or dry deposition in the boundary

5 layer en route. Recall that the corresponding air parcels spend much of the previous 7 days in the boundary layer; see Sect. 2.1.1. The decrease in [O_3] from around 50 ppbv upon initialisation to about 15 ppbv on the fight track suggests that the dry deposition of O_3 to the forest, the direct reaction of O_3 with C_5H_8 (at low ambient [NO_x]), or a combination of the two, is highly influential.

10 Comparing modelled and measured [NO], the top panel of Fig. 5 does not present a simple picture. CiTTyCAT shows reasonably good agreement at low altitudes but a tendency, at least in places, to overestimate measured [NO] at mid-to-high altitudes, perhaps contributing to its overestimation of [O_3] here. Meanwhile, UM-UKCA shows generally good agreement at higher altitudes but a tendency to overestimate [NO] in

15 and near the boundary layer, possibly contributing to its overestimation of [O_3] in these portions of the flight. The agreement between each model and the measurements for [NO_2], though imperfect, is reasonably good; see bottom panel of Fig. 5. We note that CiTTyCAT simulates higher [NO_2] than UM-UKCA shortly after 13:00 UT and, in doing so, overestimates the measurements. CiTTyCAT's underestimation of [O_3] in this

20 portion of the flight (see earlier) does not therefore appear to be due to a lack of [NO_x]. We speculate, instead, that this could be due to a lack of vertical mixing – a lack of ventilation of the boundary layer and hence exchange with free tropospheric air of higher [O_3]. Likewise, CiTTyCAT's overestimation of [O_3] in mid-to-high altitude portions of the flight could reflect a lack of vertical mixing within the free troposphere, and thus

25 the relaxation of elevated values of [O_3] (with which the air parcels are initialised; 50–90 ppbv) towards lower background concentrations. Subject to the same emissions (UKCA res), CiTTyCAT consistently simulates considerably higher [O_3] than UM-UKCA at mid-to-high altitudes: this is observed across all five flights (see Figs. S1–S4).

The measurements of $[C_5H_8]$ reflect its short lifetime with respect to oxidation by OH, reaching up to around 10 ppbv low down in the boundary layer (close to its sources) but swiftly decreasing with increasing altitude; see Fig. 6. Both models capture the rapid decrease in $[C_5H_8]$ with altitude but both tend to overestimate $[C_5H_8]$ at low altitudes with respect to the measurements, most particularly CiTTyCAT. It is possible that the C_5H_8 emissions we employ are too high but, in terms of their global annual total, they lie towards the lower end of literature estimates: 354 Tg(C) year^{-1} compared to 300–600 Tg(C) year^{-1} (e.g., Guenther et al., 2006; Arneth et al., 2008). Moreover, year-round measurements of C_5H_8 fluxes have recently been made at the TT34 site (2°35.673′ S 60°12.555′ W) in the Reserva Biologica do Cueiras in Central Amazonia, approximately 50 km north of Manaus (the destination of flight B735), as part of the Cooperative LBA Atmospheric Regional Experiment (CLAIRE-UK); "LBA" stands for Large-Scale Biosphere–Atmosphere Experiment in Amazonia. The fluxes were measured using PTR-MS and virtual disjunct eddy covariance; the site has previously been described by Martin et al. (2010). The September 2013 monthly mean (24 h average) C_5H_8 flux measured was 7.8×10^{-10} kg (C_5H_8) m^{-2} s^{-1}, with a standard deviation of 4.7×10^{-10} kg (C_5H_8) m^{-2} s^{-1} (E. House, personal communication, 2015). The possibility of inter-year variability aside, the C_5H_8 emissions we employ compare very favourably in this region, averaging 7.9×10^{-10} kg (C_5H_8) m^{-2} s^{-1} in September 2012 – the month in which all five case-study SAMBBA flights took place. Furthermore, the same emissions are used in UM-UKCA (CheT) and CiTTyCAT (CheT), so the more marked overestimation in CiTTyCAT is at least partly due to some other reason. Again, this difference between the two models extends across all five flights (see Figs. S1–S4) and we suggest that it is consistent with a lack of vertical mixing in CiTTyCAT: air parcels bound for low altitude portions of the flight are exposed to C_5H_8 emissions in the boundary layer but subject to no ventilation of the boundary layer and, hence, exchange with free tropospheric air of lower, if not zero, $[C_5H_8]$. In Sect. 3.4, we will explore the impact of introducing a simple treatment of diffusive vertical mixing in CiTTyCAT. In intervening sections, however, we first explore the effects of a change of

chemical mechanism and an increase in the resolution of trace gas emissions. The switch from CheT to CheT2 chemistry, for example, may be expected to reduce the $[C_5H_8]$ simulated in both models on account of including an OH "recycling" mechanism (see Sect. 2.3).

Finally, we compare modelled and measured [CO] in Fig. 7. Note that the high/low [CO] values at approximately one hour intervals correspond to the "span/zero" in-flight calibrations of the VUV fluorescence CO monitor (see Sect. 2.1.4). UM-UKCA generally underestimates the measurements, simulating around 100 ppbv throughout the flight; this is understood to be linked to a general high bias in [OH], and hence a low bias in CO lifetime, in this version of the model (see, e.g., Telford et al., 2013). Meanwhile, CiTTyCAT simulates near identical concentrations to UM-UKCA in the mid-to-high altitude portions of the flight, but considerably higher [CO] at low altitudes. These higher concentrations overestimate the measurements – possibly the result of overestimating $[C_5H_8]$, and hence overestimating the production of CO from C_5H_8 oxidation. A lack of boundary-layer ventilation in CiTTyCAT, and hence a lack of exchange between air with high [CO] in the boundary layer and free tropospheric air of lower [CO], could again contribute. The low bias in [CO] simulated with UM-UKCA extends across all five flights (see Figs. S1–S4); the difference in behaviour between the two models clearly extends to fights B749 and B750 (Figs. S3 and S4) but is less pronounced on flights B744 and B745 (Figs. S1 and S2).

3.2 Comparing chemical mechanisms (CheT and CheT2)

We find that the chemical mechanism employed has a negligible effect on the $[O_3]$, and only a modest effect on the [NO], $[NO_2]$, $[C_5H_8]$ and [CO], we simulate for flight B735 in UM-UKCA and CiTTyCAT (see Fig. 8). The impact of switching from CheT to CheT2 for [NO] and $[NO_2]$ is largely limited to the low altitude portions of the flight in which C_5H_8 is encountered. This is consistent with the direct changes to the chemistry being limited to ones relating to ISON (the lumped species comprised of first generation isoprene nitrates); see Sect. 2.3. To first order, we would expect the increase in the

yield of NO$_x$ from ISON in line with Perring et al. (2009) and the addition of O$_3$-initiated ISON degradation (Lockwood et al., 2010) to increase [NO$_x$]. We find that the CheT2 chemistry generally yields slightly higher [NO] and [NO$_2$] in CiTTyCAT but slightly lower [NO] and [NO$_2$] in UM-UKCA; the impact in both models, however, is modest. In these same portions of the flight, [C$_5$H$_8$] and [CO] decrease on switching from CheT to CheT2 chemistry – in both models. The decrease in [C$_5$H$_8$] is presumably the result of introducing OH regeneration via the formation of HPALDS from ISO$_2$ and their subsequent rapid release of OH (Peeters et al., 2009; Crounse et al., 2011); see, again, Sect. 2.3. However, CiTTyCAT's overestimation of [C$_5$H$_8$] relative to UM-UKCA (and the measurements) is little reduced. Meanwhile, the decrease in [CO], negligible in UM-UKCA but noticeable in CiTTyCAT, suggests that the increased rate of CO removal by OH (as a result of OH regeneration) at least compensates for the increased rate of CO production from C$_5$H$_8$ oxidation (and the oxidation of CH$_4$ and other NMVOCs). It is possible that the "smearing out" of NO$_x$ emissions at 3.75° × 2.5°, in the integrations examined thus far, yields few regions of sufficiently low [NO$_x$] for effective OH regeneration; we explore the impact of employing "High res" emissions in the next section.

On the other four flights, the switch to CheT2 chemistry has a negligible effect on the simulations with UM-UKCA; see Figs. S5–S8. In CiTTyCAT, the reduction in [C$_5$H$_8$] remains modest for flights B744 and B745 (Figs. S5 and S6) but is larger for flights B749 and B750 (Figs. S7 and S8); the increase in [NO] and [NO$_2$] simulated with CiTTyCAT are also greater for the latter two flights, and [O$_3$] demonstrates sensitivity to the chemical mechanism employed during some portions of flight B750 too. The difference in [C$_5$H$_8$] simulated with CiTTyCAT and UM-UKCA, however, remains large, and we remain interested in the impact of vertical mixing.

3.3   Comparing trace gas emissions of different resolutions

Switching from "UKCA res" to "High res" emissions also has negligible effect on the [O$_3$] we simulate for flight B735 in CiTTyCAT, everywhere but the beginning and end of the flight; see Fig. 9. At either end of the flight, the higher [O$_3$] simulated subject to

Title Page

Abstract   Introduction

Conclusions   References

Tables   Figures

◀   ▶

◀   ▶

Back   Close

Full Screen / Esc

Printer-friendly Version

Interactive Discussion

High res emissions (irrespective of the chemical mechanism employed) is presumably attributable to the latter's greater ability to resolve elevated emissions of O_3 precursors associated with the respective cities/airports (Porto Velho and Manaus). As with the change of chemical mechanism explored in the last section, the increase in emission resolution has only a modest effect of the [NO], [NO_2] and [CO] we simulate, and is limited to the low altitude portions of the flight – in which the corresponding air parcels have spent much of the last 7 days in the boundary layer exposed to emissions. Whilst the High res emissions yield lower [C_5H_8] (again irrespective of the chemical mechanism employed), CiTTyCAT continues to greatly overestimate [C_5H_8] relative to the measurements and the difference in [C_5H_8] simulated with the two models is reduced but not removed; for clarity, the [C_5H_8] simulated with UM-UKCA is not included in Fig. 9 (please refer back to Fig. 8).

A different story emerges for the other four flights; see Figs. S9–S12. [C_5H_8], simulated subject to both CheT and CheT2 chemistries, decreases markedly: practically to zero on flights B744 and B745 (Figs. S9 and S10), now actually underestimating the measurements; and, though still overestimating, much closer in line with the measurements on flights B749 and B750 (Figs. S11 and S12). Furthermore, the [O_3] simulated, again subject to both CheT and CheT2 chemistries, changes considerably. Notably, at mid-to-high altitudes, CiTTyCAT's overestimation of the measurements is much reduced on flights B744, B749 and B750 (Figs. S9, S10 and S12) and largely removed on flight B745 (Fig. S10). So, in this one regard – the insensitivity our simulations show to the resolution of trace gas emissions employed – flight B735 appears to be an exception. Remember, however, that we explore the impact of emission resolution in the Lagrangian environment alone, where we can exploit a resolution of 0.1° × 0.1°; this would be computationally infeasible in an Eulerian chemistry-climate model run globally. Moreover, what does not change is that, in otherwise directly comparable experiments with UM-UKCA and CiTTyCAT (employing emissions of the same resolution, and the same chemical mechanism), the Lagrangian model yields much higher [O_3] at mid-to-high altitudes, and much higher [C_5H_8] at low altitudes, than the Eulerian model.

We observe this behaviour across all five case study flights, and it is this central finding, which appears to result from the choice of model framework alone, on which we mean to focus from here on and speculate is the result of differences in vertical mixing.

3.4 Exploring sensitivity to vertical mixing in CiTTyCAT

To explore the impact of introducing a simple treatment of diffusive vertical mixing in the Lagrangian framework, we return to flight B735, employing "UKCA res" emissions and CheT chemistry. We explore three formulations of mixing, or relaxation, as outlined in Sect. 2.2.2 and Table 1: Mix1, Mix2 and Mix3. These formulations differ with respect to the timescales on which the concentrations of species simulated in CiTTyCAT are relaxed towards background concentrations in the free troposphere (τ_{FT}) and boundary layer (τ_{BL}), increasing from Mix1 to Mix3 commensurate with increasingly stable conditions; see, again, Table 1. The three formulations can be caricatured as follows: Mix1 (solid red line) applies rapid relaxation in both regions; Mix2 (solid blue line) applies slower relaxation in both regions; and Mix3 (solid green line) applies the same, relatively slow relaxation in the boundary layer as Mix2 but still slower relaxation in the free troposphere. The picture regarding [NO] is not simple to summarise. However, for [O_3], [NO_2], [C_5H_8] an [CO], the inclusion of this relaxation, subject to all three formulations (Mix1–3), brings the concentrations simulated with CiTTyCAT, originally with no mixing (dotted green lines), much closer in line with those simulated with UM-UKCA (dashed blue lines). It would therefore appear that vertical mixing (or the lack thereof) has potential to explain some of the differences observed between the two models/model frameworks.

Of course, the close agreement between UM-UKCA and CiTTyCAT, on including mixing in the latter, is only to be expected for [O_3], since we relax the [O_3] simulated with CiTTyCAT towards monthly mean values simulated with UM-UKCA (see Sect. 2.2.2). We do likewise for other species of intermediate lifetimes: CO, C_2H_6, C_3H_8 and PAN. Meanwhile, the concentrations of all short-lived species, including C_5H_8, are relaxed towards zero concentrations – characteristic of free tropospheric air. The most rapid

relaxation, Mix1, yields the best agreement between modelled and measured $[C_5H_8]$. Indeed, the agreement is excellent. However, Mix1 yields the worst agreement between modelled and measured $[O_3]$ in the low altitude portions of the flight – in these regions, considerably worse than the simulation without mixing, consistently overestimating the measurements by 15–20 ppbv in absolute terms, and close to 100 % in relative terms. The slower relaxations, Mix 2 and Mix 3, yield somewhat higher $[C_5H_8]$ – greater than that measured but a significant improvement over that simulated with CiTTyCAT without mixing, and better in two out of three portions of the flight than that simulated with UM-UKCA. Mix2 and Mix3, meanwhile, yield better agreement between modelled and measured $[O_3]$ in the low altitude parts of the flight. Furthermore, Mix3 starts to retain some of the structure in $[O_3]$ simulated in the high altitude portions of the flight that is almost entirely absent from the simulation with UM-UKCA but present, at least to some extent, in the measurements; see earlier discussion in Sect. 3.1. Judging by the structure present in the $[O_3]$ measured in these parts of the flight, there could be justification for still slower relaxation in the free troposphere. The mixing formulation could be iterated further, however, of the three formulations applied here (exploring the range of parameter values suggested in the literature; see Sect. 2.2.2 and Table 1), we judge Mix3 to be the most appropriate overall.

3.5 Modelling atmospheric chemistry downwind of Manaus

We now move from what has predominantly been an exploration in the spatial domain – in other words, comparing modelled and measured trace gas concentrations on flight tracks – to an exploration of the temporal domain. We simulate $[O_3]$ at a single site downwind of Manaus over an extended period of time, the month in which all five case-study SAMBBA flights took place. Recall, back-trajectories were calculated from a boundary layer site (61.0° W, 3.1° S, 900 hPa) roughly 100 km downwind (1° west) of Manaus at 6 hourly intervals throughout September 2012. The choice of site is arbitrary; we are not aware of any measurements of $[O_3]$ at this site or comparable sites, during the period in question, with which to compare the $[O_3]$ we simulate –

this is a purely model-based exploration of the consequences of simulating boundary layer [O_3] with an Eulerian model run in "climate mode" (UM-UKCA) and a Lagrangian model capable of exploiting very high resolution anthropogenic emissions and retaining compositional structure (CiTTyCAT).

⁵ The structure that Lagrangian modelling can generate in [O_3], and retain over a period of time, is of particular interest in an exploration of the exposure to boundary-layer [O_3] of the rainforest downwind of an isolated source such as Manaus. Plant exposure to ozone is often expressed in terms of accumulated exposure above a given threshold. For crop species, the most commonly used metric remains the total number of hour-

¹⁰ averages over 40 ppbv accumulated over a 3 month growing season, AOT40 (UNECE, 2010), although there is growing awareness that plant effects are more closely linked to the stomatal ozone dose than concentration exposure, such as the phytotoxic O_3 dose above a threshold flux Y (POD$_Y$; see, e.g., LRTAP Convention, 2010). For tropical, long-lived, wild plants, such as those in the rainforest downwind of Manaus, the "grow-

¹⁵ ing season" may not be the appropriate accumulation time (Ainsworth et al., 2012). Below, we discuss an AOT40-like exposure metric based on a 30 day time series, and refer to the metric as "AOT40" to remind readers of the non-standard accumulation period we use. Our study is not designed to calculate annual exposure metrics, but simply to highlight the sensitivity of exposure metrics to the modelling method used

²⁰ (where measurements are not available). In view of the sensitivity that our simulations with CiTTyCAT show to the inclusion of a simple treatment of diffusive vertical mixing (relaxation towards background composition; see previous section), we simulate the [O_3] downwind of Manaus with and without relaxation formulations, Mix1–3. We start, as before, by using CheT chemistry but employ High res emissions (0.1° × 0.1°)

²⁵ in an attempt to resolve the episodic influence of anthropogenic emissions from the city 100 km upwind. We compare the results of these integrations with the [O_3] simulated with UM-UKCA in "climate mode" (employing anthropogenic emissions at 3.75° × 2.5°) in the top left of Fig. 11; the corresponding "box and whisker" plots of the absolute min-

imum, absolute maximum, median, and 25th and 75th percentile values of simulated [O_3] are included in the top right.

In the absence of vertical mixing, the [O_3] simulated with CiTTyCAT (dotted green line) exhibits much more structure than that simulated with UM-UKCA (dashed blue line), frequently exceeding 50 ppbv and exceeding 75 ppbv on seven occasions. Depending on the speed of relaxation imposed, this structure is suppressed to a greater or lesser extent, and the simulations with CiTTyCAT (solid red, blue and green lines) can generate more or less variability in the time series than UM-UKCA. Mixing formulation, Mix3, judged in the last section to yield best agreement between modelled and measured [O_3] over a range of altitudes, including specifically low altitudes, yields a distribution of [O_3] that has a higher median value than UM-UKCA (34.0 cf. 31.7 ppbv), a higher 75th percentile (38.3 cf. 34.9 ppbv), and a higher absolute maximum (54.3 cf. 41.7 ppbv). The [O_3] simulated with UM-UKCA never exceeds 50 ppbv in this period, whilst that simulated with CiTTyCAT, subject to Mix3, does so five times. This shift towards higher [O_3] leads to an 8 % increase in mean [O_3] simulated throughout the month, from 32.5 to 35.1 ppbv. Note that the "AOT40" we calculate over just 30 days increases by a factor of almost 40, from 22.6 to 863 ppbv h.

In the bottom left of Fig. 11, we explore the effects on the simulation of [O_3] with CiTTyCAT, subject to Mix3, of changing from CheT to CheT2 chemistry and/or degrading the resolution of the emissions to that used in UM-UKCA ($3.75° \times 2.5°$); the corresponding box and whisker plots are included in the bottom right. Only modest differences arise. The switch to CheT2 chemistry yields substantially different [O_3] only on two days (21 and 24 September); compare the green and red lines. Meanwhile, degrading the resolution of the emissions has little effect throughout; compare the solid and dotted lines. Our earlier findings appear to hold irrespective of the chemistry and emissions employed: CiTTyCAT (Mix3) yields much more structure in [O_3] than UM-UKCA, exceeding 50 ppbv on four or five occasions as opposed to none; and, whilst the mean [O_3] increases by approximately 10 %, or 3 ppbv, "AOT40" increases by a factor of roughly 40–60; see Table 4. Whilst our study was not designed to calculate flux-based

ozone metrics, such as POD_Y (see above), we would expect a less marked difference in the latter; it would depend, however, on how peak $[O_3]$ values correlate with turbulence and plant physiology (e.g. stomatal opening).

The broader message is that all three metrics investigated here change on moving from a global chemistry-climate model run in "climate mode" to a combination of this model and a Lagrangian model capable of exploiting very high resolution anthropogenic emissions and retaining compositional structure. The combination of models may yield a not-dissimilar background exposure, but one punctuated episodically with acute, high $[O_3]$ events. It is interesting that this does not appear to be the result of the Lagrangian model's ability to exploit very high resolution anthropogenic emissions, despite the site being just 100 km downwind of Manaus; recall, this insensitivity was observed in our simulations of flight B735, bound for Manaus. Instead, it appears to be the result of its ability to retain heterogeneity in the origins of air parcels, and their histories over the previous seven days.

4   Summary and discussion

We have confronted two atmospheric chemistry models – a global Eulerian chemistry-climate model, UM-UKCA (Hewitt et al., 2011; O'Connor et al., 2014), and a trajectory-based Lagrangian model, CiTTyCAT (Pugh et al., 2012) – with airborne measurements of atmospheric composition above the Amazon rainforest (O_3, NO, NO_2, C_5H_8 and CO) from the 2012 SAMBBA campaign (see Darbyshire and Johnson, 2013). To our surprise, the simulations with the two models proved relatively insensitive to the chemical mechanism employed (CheT or CheT2; see Sects. 3.2 and 3.5). Explored only in the Lagrangian environment, the sensitivity our simulations showed to the spatial resolution of trace gas emissions ($0.1° \times 0.1°$ and $3.75° \times 2.5°$; see Sects. 3.3 and 3.5) varied from one flight to another, and from one chemical species to another. However, what proved highly influential, in otherwise directly comparable experiments across all five case study flights, was the choice of model framework itself. We believe this

was the result of the different treatments of transport in the two model frameworks, and their consequences for mixing (see Sect. 3.1). The lack of explicit mixing in the Lagrangian model yielded structure in its simulations of atmospheric composition, particularly [O_3], that was more reminiscent of that largely (but not always) exhibited by the measurements, though perhaps a little too pronounced. Meanwhile, extensive mixing in the Eulerian model removed much of this structure but yielded better overall agreement with the measurements in terms of magnitude (see Sect. 3.1). We found a simple treatment of mixing – relaxing the composition of air parcels in the Lagrangian model towards monthly mean data from the Eulerian model – to offer a compromise between the two, combining some of the benefits of both. Applied to the simulation of boundary layer [O_3], we showed that the choice of model framework affects our understanding of both the frequency at which the rainforest is exposed to damaging [O_3] and the duration for which it is so exposed, as quantified for example in terms of a version of the accumulation-over-threshold metric, AOT40 (see Sect. 3.5).

We noted in the introduction that Lagrangian models, run in "domain-filling" mode, capture much of the strain-induced stirring of the atmosphere, with no mixing, whilst Eulerian models capture the large-scale stirring but inevitably introduce mixing as they average concentrations across grid boxes (see, e.g., Dragani et al., 2002; Methven et al., 2003). The Lagrangian model thus, predictably, proved capable of retaining much more structure than the Eulerian model: heterogeneity in the chemical composition of air parcels bound for points spaced only a few minutes apart along a flight track, or arriving at the same location at regular intervals (every 6 h) over an extended period of time. We found that this additional structure largely reflected the model's ability to resolve the different origins of air parcels (7 days previously) and, only to a lesser extent, differences in: the routes by which they were subsequently transported; the emissions and deposition to which they were exposed en route; and hence the chemistry that took place within them. The composition of each air parcel was simulated independently in the Lagrangian model (i.e. assuming no mixing took place between them). There was not only no mixing in the horizontal, but no mixing in the vertical; the Lagrangian model

included neither explicit vertical mixing in the boundary layer (due to convection) nor ventilation of the boundary layer and exchange with air in the free troposphere. It is to the latter that we attribute the Lagrangian model's overestimation of $[C_5H_8]$ in the boundary layer and $[O_3]$ in the free troposphere; we believe they are the result of a lack

5 of mixing with, and hence dilution by, lower $[C_5H_8]$ air above and lower $[O_3]$ air below respectively (see Sect. 3.1 and, earlier, Sect. 2.2.2).

The simple approach to diffusive vertical mixing that we later introduced into the Lagrangian model has been used in previous studies; see Pugh et al. (2012) and the references contained therein. It comprised: the relaxation of species of "intermediate

10 lifetimes" towards 3-D monthly mean concentrations simulated in the Eulerian model; and the relaxation of short-lived species (all other species besides CH_4) towards zero concentrations (characteristic of the free troposphere). Recall that $[CH_4]$ was fixed in the model. The relaxation was applied on timescales τ_{BL} and τ_{FT} in the boundary layer and free troposphere respectively; see Sect. 2.2.2 and Table 1 for more details. Having

15 explored just three combinations of τ_{BL} and τ_{FT} spanning literature values, we cannot claim to have fully optimised this simple treatment of mixing. Predictably, however, all three formulations brought the Lagrangian simulations more closely in line with their Eulerian counterparts; see Sect. 3.5. Moreover, one formulation, Mix3 ($\tau_{BL} = 27.8$ h, subject to a boundary layer height of 1000 m, and $\tau_{FT} = 69.4$ h) yielded the desirable

20 combination of: reasonable agreement with measurements of both $[O_3]$ and $[C_5H_8]$ at low altitudes; and structure in the simulated $[O_3]$ reminiscent of that exhibited by the measurements. It was predominantly this formulation that we subsequently applied to a simulation of boundary layer $[O_3]$.

We should note at this point that the $[O_3]$ simulated by this combination of Lagrangian

25 and Eulerian models (subject to Mix3) did not show as good agreement with the measurements at low altitudes as that simulated with the Lagrangian model alone: the Lagrangian model simulated 10–15 ppbv lower $[O_3]$ than the combination of models (and the Eulerian model on its own), in closer agreement with the measurements. It may have done so, however, for the wrong reason. If the lack of vertical mixing in the

Lagrangian model contributed to its overestimation of [O$_3$] in the free troposphere, it likely also contributed to its simulation of low [O$_3$] in the boundary layer; the lack of ventilation of the boundary layer, and exchange with free tropospheric air aloft, would have neglected mixing with, and enrichment by, higher [O$_3$] air above. This raises the question whether something else might be amiss in the model(s), leading to an over-estimation of boundary layer [O$_3$] in this environment. One possibility is that the dry deposition of O$_3$ to the rainforest is underestimated. Hardacre et al. (2015) recently highlighted the crude treatment of dry deposition to tropical forests in current global chemistry-climate models. In both the Lagrangian model and the Eulerian model, we have employed a 1 m dry deposition velocity (V_d) of 0.5 cm s^{-1} to the forest. This com-pares favourably with the measurements of Rummel et al. (2007) in the Amazon, which yielded a "mean midday maximum" O$_3$ V_d of 0.5 cm s^{-1} in the dry season. However, such measurements in the Amazon are sparse and the V_d of O$_3$ could vary from one region to another: more O$_3$ V_d measurements are called for.

We used the Lagrangian model, the Eulerian model, and the combination of the two models, to simulate [O$_3$] at a site in the boundary layer, approximately 100 km downwind of Manaus, over a period of a month; see Sect. 3.5. The choice of site was arbitrary, but chosen in anticipation of demonstrating the need to employ very high resolution anthropogenic emissions (capable of resolving a city of the order of 10 km × 10 km) to correctly capture the chemistry and composition downwind. To our surprise, our simulations again proved relatively insensitive to the resolution of emis-sions (and chemical mechanism) employed, consistent with our earlier findings when simulating the SAMBBA measurements. However, again, they demonstrated a high degree of sensitivity to the model framework; see top left and top right of Fig. 11. At one extreme, the Lagrangian model yielded very high variability in [O$_3$] at this site, fre-quently exceeding 50 ppbv and sometimes exceeding 75 ppbv. At the other extreme, the Eulerian model simulated far less variability in [O$_3$], never exceeding 50 ppbv and yielding a mean [O$_3$] of 32.5 ppbv and an "AOT40" of around 20 ppbv h (over 30 days). Between these extremes, the combination of Lagrangian and Eulerian models (subject

to Mix3), yielded [O_3] of intermediate variability, exceeding 50 ppbv on four or five occasions. Compared to the Eulerian model, it generated only a 10 % higher mean [O_3], of 35–36 ppbv, but an "AOT40" approximately 50 times greater, of the order of 1000 ppbv h (over 30 days). The key message here is that both the frequency at which the rainforest is exposed to damaging [O_3], and the duration for which it is so exposed, change with the model framework. The choice of model framework therefore has a strong bearing on predictions of the exposure of tropical forests to ground-level ozone, and hence our understanding of the health of the rainforest, the tropical carbon cycle, and how these might change under future climate- and trace gas emission scenarios. It is not clear from the current time series study whether it is possible to derive a transfer function by which to modify chemistry-climate simulations of ozone over tropical rainforest, but our results clearly motivate a further study to seek such a function.

The Supplement related to this article is available online at doi:10.5194/acpd-15-24251-2015-supplement.

for Atmospheric Science, University of Cambridge, for their generous welcome whilst working remotely there as a visiting researcher.

References

Ainsworth, E. A., Yendrek, C. R., Sitch, S., Collins, W. J., and Emberson, L. D.: The effects of tropospheric ozone on net primary productivity and implications for climate change, Annu. Rev. Plant Biol., 63, 637–61, 2012.

Archibald, A. T., Cooke, M. C., Utembe, S. R., Shallcross, D. E., Derwent, R. G., and Jenkin, M. E.: Impacts of mechanistic changes on HO_x formation and recycling in the oxidation of isoprene, Atmos. Chem. Phys., 10, 8097–8118, doi:10.5194/acp-10-8097-2010, 2010a.

Archibald, A. T., Jenkin, M. E., and Shallcross, D. E.: An isoprene mechanism intercomparison, Atmos. Environ., 44, 5356–5364, doi:10.1016/j.atmosenv.2009.09.016, 2010b.

Arneth, A., Monson, R. K., Schurgers, G., Niinemets, Ü., and Palmer, P. I.: Why are estimates of global terrestrial isoprene emissions so similar (and why is this not so for monoterpenes)?, Atmos. Chem. Phys., 8, 4605–4620, doi:10.5194/acp-8-4605-2008, 2008.

Avnery, S., Mauzerall, D., Liu, J., and Horowitz, L.: Global crop yield reductions due to surface ozone exposure: 1. Year 2000 crop production losses and economic damage, Atmos. Environ., 45, 2284–2296, 2011.

Beerling, D. and Woodward, F.: Vegetation and the Terrestrial Carbon Cycle: The First 400 Million Years, Cambridge University Press, Cambridge, UK, p. 405, 2001.

Beerling, D., Woodward, F., Lomas, M., and Jenkins, A.: Testing the responses of a dynamic global vegetation model to environmental change: a comparison of observations and predictions, Global Ecol. Biogeogr., 6, 439–450, 1997.

Butler, T. M., Taraborrelli, D., Brühl, C., Fischer, H., Harder, H., Martinez, M., Williams, J., Lawrence, M. G., and Lelieveld, J.: Improved simulation of isoprene oxidation chemistry with the ECHAM5/MESSy chemistry-climate model: lessons from the GABRIEL airborne field campaign, Atmos. Chem. Phys., 8, 4529–4546, doi:10.5194/acp-8-4529-2008, 2008.

Cain, M., Methven, J., and Highwood, E. J.: Quantification of chemical and physical processes influencing ozone during long-range transport using a trajectory ensemble, Atmos. Chem. Phys., 12, 7015–7039, doi:10.5194/acp-12-7015-2012, 2012.

Title Page

Abstract | Introduction

Conclusions | References

Tables | Figures

◀ | ▶|

◀ | ▶

Back | Close

Full Screen / Esc

Printer-friendly Version

Interactive Discussion

Carlton, A. G., Wiedinmyer, C., and Kroll, J. H.: A review of Secondary Organic Aerosol (SOA) formation from isoprene, Atmos. Chem. Phys., 9, 4987–5005, doi:10.5194/acp-9-4987-2009, 2009.

Chen, Q., Farmer, D. K., Rizzo, L. V., Pauliquevis, T., Kuwata, M., Karl, T. G., Guenther, A., Allan, J. D., Coe, H., Andreae, M. O., Pöschl, U., Jimenez, J. L., Artaxo, P., and Martin, S. T.: Submicron particle mass concentrations and sources in the Amazonian wet season (AMAZE-08), Atmos. Chem. Phys., 15, 3687–3701, doi:10.5194/acp-15-3687-2015, 2015.

Crounse, J. D., Paulot, F., Kjaergaard, H. G., and Wennberg, P. O.: Peroxy radical isomerization in the oxidation of isoprene, Phys. Chem. Chem. Phys., 13, 13607–13613, 2011.

Crowther, R., Law, K., Pyle, J., Bekki, S., and Smit, H.: Characterising the effect of large-scale model resolution upon calculated OH production using MOZAIC data, Geophys. Res. Lett., 29, 1613, doi:10.1029/2002GL014660, 2002.

Darbyshire, E. and Johnson, B.: The South American Biomass Burning Analysis (SAMBBA) Field Experiment, September–October 2012, Brazil: Summary of research flights (available on request from the authors), University of Manchester, Manchester, UK, and UK Met Office, Exeter, UK, 2013.

Dodge, M.: Combined use of modeling techniques and smog chamber data to derive ozone-precursor relationships, in: Proceedings of the International Conference on Photochemical Oxidant Pollution and its Control, United States Environmental Protection Agency, 12–17 September 1976, Raleigh, North Carolina, USA, 881–889, 1977.

Dragani, R., Redaelli, G., Visconti, G., Mariotti, A., Rudakov, V., MacKenzie, A. R., and Stefanutti, L.: High resolution stratospheric tracer fields reconstructed with lagrangian techniques: a comparative analysis of predictive skill, J. Atmos. Sci., 59, 1943–1958, 2002.

European Commission, Joint Research Centre (JRC)/Netherlands Environmental Assessment Agency (PBL): Emission Database for Global Atmospheric Research (EDGAR), release version 4.0, available at: http://edgar.jrc.ec.europa.eu (last access: January 2015), 2009.

Evans, M. J., Shallcross, D. E., Law, K. S., Wild, J. O. F., Simmonds, P. G., Spain, T. G., Berrisford, P., Methven, J., Lewis, A. C., McQuaid, J. B., Pilling, M. J., Bandy, B. J., Penkett, S. A., and Pyle, J. A.: Evaluation of a Lagrangian box model using field measurements from EASE (Eastern Atlantic Summer Experiment) 1996, Atmos. Environ., 34, 3843–3863, 2000.

Gerbig, C., Schmitgen, S., Kley, D., and Volz-Thomas, A.: An improved fast-response vacuum-UV resonance fluorescence CO instrument, J. Geophys. Res., 104, 1699–1704, doi:10.1029/1998jd100031, 1999.

Title Page

Abstract | Introduction

Conclusions | References

Tables | Figures

|◄ | ►|

◄ | ►

Back | Close

Full Screen / Esc

Printer-friendly Version

Interactive Discussion

Gregory, D. and Allen, S.: The effect of convective downdraughts upon NWP and climate simulations, in: Nineth Conference on Numerical Weather Prediction, Denver, Colorado, 122–123, 1991.

Gregory, D. and Rowntree, P. R.: A massflux convection scheme with representation of cloud ensemble characteristics and stability dependent closure, Mon. Weather Rev., 118, 1483–1506, 1990.

Guenther, A., Hewitt, C., Erickson, D., Fall, R., Geron, C., Graedel, T., Harley, P., Klinger, L., Lerdau, M., McKay, W., Pierce, T., Scholes, B., Steinbrecher, R., Tallamraju, R., Taylor, J., and Zimmerman, P.: A global model of natural volatile organic compound emissions, J. Geophys. Res., 100, 8873–8892, 1995.

Guenther, A., Karl, T., Harley, P., Wiedinmyer, C., Palmer, P. I., and Geron, C.: Estimates of global terrestrial isoprene emissions using MEGAN (Model of Emissions of Gases and Aerosols from Nature), Atmos. Chem. Phys., 6, 3181–3210, doi:10.5194/acp-6-3181-2006, 2006.

Guenther, A. B., Jiang, X., Heald, C. L., Sakulyanontvittaya, T., Duhl, T., Emmons, L. K., and Wang, X.: The Model of Emissions of Gases and Aerosols from Nature version 2.1 (MEGAN2.1): an extended and updated framework for modeling biogenic emissions, Geosci. Model Dev., 5, 1471–1492, doi:10.5194/gmd-5-1471-2012, 2012.

Hardacre, C., Wild, O., and Emberson, L.: An evaluation of ozone dry deposition in global scale chemistry climate models, Atmos. Chem. Phys., 15, 6419–6436, doi:10.5194/acp-15-6419-2015, 2015.

Hewitt, C. N., Lee, J. D., MacKenzie, A. R., Barkley, M. P., Carslaw, N., Carver, G. D., Chappell, N. A., Coe, H., Collier, C., Commane, R., Davies, F., Davison, B., DiCarlo, P., Di Marco, C. F., Dorsey, J. R., Edwards, P. M., Evans, M. J., Fowler, D., Furneaux, K. L., Gallagher, M., Guenther, A., Heard, D. E., Helfter, C., Hopkins, J., Ingham, T., Irwin, M., Jones, C., Karunaharan, A., Langford, B., Lewis, A. C., Lim, S. F., MacDonald, S. M., Mahajan, A. S., Malpass, S., McFiggans, G., Mills, G., Misztal, P., Moller, S., Monks, P. S., Nemitz, E., Nicolas-Perea, V., Oetjen, H., Oram, D. E., Palmer, P. I., Phillips, G. J., Pike, R., Plane, J. M. C., Pugh, T., Pyle, J. A., Reeves, C. E., Robinson, N. H., Stewart, D., Stone, D., Whalley, L. K., and Yin, X.: Overview: oxidant and particle photochemical processes above a south-east Asian tropical rainforest (the OP3 project): introduction, rationale, location characteristics and tools, Atmos. Chem. Phys., 10, 169–199, doi:10.5194/acp-10-169-2010, 2010.

Title Page

Abstract | Introduction

Conclusions | References

Tables | Figures

|◄ | ►|

◄ | ►

Back | Close

Full Screen / Esc

Printer-friendly Version

Interactive Discussion

Hewitt, H. T., Copsey, D., Culverwell, I. D., Harris, C. M., Hill, R. S. R., Keen, A. B., McLaren, A. J., and Hunke, E. C.: Design and implementation of the infrastructure of HadGEM3: the next-generation Met Office climate modelling system, Geosci. Model Dev., 4, 223–253, doi:10.5194/gmd-4-223-2011, 2011.

Hopkins, J. R., Jones, C. E., and Lewis, A. C.: A dual channel gas chromatograph for atmospheric analysis of volatile organic compounds including oxygenated and monoterpene compounds, J. Environ. Monitor., 13, 2268–2276, 2011.

IPCC, Climate change 2001: The scientific basis. Contribution of Working Group 1 to the Third Assessment Report of the Intergovernmental Panel on Climate Change, edited by: Houghton, J. T., Ding, Y., Griggs, D. J., Noguer, M., van der Linden, P. J., Dai, X., Maskell, K., and Johnson, C. A., Cambridge University Press, Cambridge, UK, and New York, USA, doi:10.1002/joc.763, 2002.

Jenkin, M.: Review of the atmospheric chemistry of isoprene and evaluation of mechanisms for global modelling, Tech. Rep., UK Met Office, Atmospheric Chemistry Services, Oakhampton, Devon, UK, 2012.

Jenkin, M. E., Saunders, S. M., and Pilling, M. J.: The tropospheric degradation of volatile organic compounds: a protocol for mechanism development, Atmos. Environ., 31, 81–104, 1997.

Krol, M., Molemaker, M., and de Arellano, J.: Effects of turbulence and heterogeneous emissions on photochemically active species in the convective boundary layer, J. Geophys. Res., 105, 6871–6884, 2000.

Kuhn, U., Ganzeveld, L., Thielmann, A., Dindorf, T., Schebeske, G., Welling, M., Sciare, J., Roberts, G., Meixner, F. X., Kesselmeier, J., Lelieveld, J., Kolle, O., Ciccioli, P., Lloyd, J., Trentmann, J., Artaxo, P., and Andreae, M. O.: Impact of Manaus City on the Amazon Green Ocean atmosphere: ozone production, precursor sensitivity and aerosol load, Atmos. Chem. Phys., 10, 9251–9282, doi:10.5194/acp-10-9251-2010, 2010.

Lathière, J., Hauglustaine, D. A., Friend, A. D., De Noblet-Ducoudré, N., Viovy, N., and Folberth, G. A.: Impact of climate variability and land use changes on global biogenic volatile organic compound emissions, Atmos. Chem. Phys., 6, 2129–2146, doi:10.5194/acp-6-2129-2006, 2006.

Lathière, J., Hewitt, C. N., and Beerling, D. J.: Sensitivity of isoprene emissions from the terrestrial biosphere to 20th century changes in atmospheric CO_2 concentration, climate, and land use, Glob. Change Biol., 24, GB1004, doi:10.1029/2009GB003548, 2010.

Title Page

Abstract | Introduction

Conclusions | References

Tables | Figures

|◀ | ▶|

◀ | ▶

Back | Close

Full Screen / Esc

Printer-friendly Version

Interactive Discussion

Lee, J. D., Moller, S. J., Read, K. A., Lewis, A. C., Mendes, L., and Carpenter, L. J.: Year-round measurements of nitrogen oxides and ozone in the tropical North Atlantic marine boundary layer, J. Geophys. Res., 114, D21302, doi:10.1029/2009JD011878, 2009.

Lelieveld, J., Butler, T. M., Crowley, J. N., Dillon, T. J., Fischer, H., Ganzeveld, L., Harder, H., Lawrence, M. G., Martinez, M., Taraborrelli, D., and Williams, J.: Atmospheric oxidation capacity sustained by a tropical forest, Nature, 452, 737–740, doi:10.1038/nature06870, 2008.

Lidster, R. T., Hamilton, J. F., Lee, J. D., Lewis, A. C., Hopkins, J. R., Punjabi, S., Rickard, A. R., and Young, J. C.: The impact of monoaromatic hydrocarbons on OH reactivity in the coastal UK boundary layer and free troposphere, Atmos. Chem. Phys., 14, 6677–6693, doi:10.5194/acp-14-6677-2014, 2014.

Lockwood, A. L., Shepson, P. B., Fiddler, M. N., and Alaghmand, M.: Isoprene nitrates: preparation, separation, identification, yields, and atmospheric chemistry, Atmos. Chem. Phys., 10, 6169–6178, doi:10.5194/acp-10-6169-2010, 2010.

LRTAP Convention: Chapter 3 of the LRTAP Convention Manual of Methodologies for Modelling and Mapping Effects of Air Pollution, edited by: Mills, G., Pleijel, H., Büker, P., Braun, S., Emberson, L., Harmens, H., Simpson, D., Grünhage, L., Karlsson, P., Danielsson, H., Bermejo, V., and Gonzalez-Fernandez, I., available at: http://icpvegetation.ceh.ac.uk/ (last access: 19 January 2015), 2010.

Martin, S. T., Andreae, M. O., Althausen, D., Artaxo, P., Baars, H., Borrmann, S., Chen, Q., Farmer, D. K., Guenther, A., Gunthe, S. S., Jimenez, J. L., Karl, T., Longo, K., Manzi, A., Müller, T., Pauliquevis, T., Petters, M. D., Prenni, A. J., Pöschl, U., Rizzo, L. V., Schneider, J., Smith, J. N., Swietlicki, E., Tota, J., Wang, J., Wiedensohler, A., and Zorn, S. R.: An overview of the Amazonian Aerosol Characterization Experiment 2008 (AMAZE-08), Atmos. Chem. Phys., 10, 11415–11438, doi:10.5194/acp-10-11415-2010, 2010.

Methven, J.: Offline trajectories: calculation and accuracy, Tech. Rep. UK Univ. Global Atmos. Modell. Program, Program, Dep. of Meteorol., Univ. of Reading, Reading, UK, 1997.

Methven, J., Arnold, S. R., O'Connor, F. M., Barjat, H., Dewey, K., Kent, J., and Brough, N.: Estimating photochemically produced ozone throughout a domain using flight data and a Lagrangian model, J. Geophys. Res., 108, 4271, doi:10.1029/2002JD002955, 2003.

Murphy, J. G., Oram, D. E., and Reeves, C. E.: Measurements of volatile organic compounds over West Africa, Atmos. Chem. Phys., 10, 5281–5294, doi:10.5194/acp-10-5281-2010, 2010.

Title Page

Abstract | Introduction

Conclusions | References

Tables | Figures

Back | Close

Full Screen / Esc

Printer-friendly Version

Interactive Discussion

O'Connor, F. M., Johnson, C. E., Morgenstern, O., Abraham, N. L., Braesicke, P., Dalvi, M., Folberth, G. A., Sanderson, M. G., Telford, P. J., Voulgarakis, A., Young, P. J., Zeng, G., Collins, W. J., and Pyle, J. A.: Evaluation of the new UKCA climate-composition model – Part 2: The Troposphere, Geosci. Model Dev., 7, 41–91, doi:10.5194/gmd-7-41-2014, 2014.

Pacifico, F., Folberth, G. A., Sitch, S., Haywood, J. M., Rizzo, L. V., Malavelle, F. F., and Artaxo, P.: Biomass burning related ozone damage on vegetation over the Amazon forest: a model sensitivity study, Atmos. Chem. Phys., 15, 2791–2804, doi:10.5194/acp-15-2791-2015, 2015.

Paulot, F., Crounse, J. D., Kjaergaard, H. G., Kuerten, A., St Clair, J. M., Seinfeld, J. H., and Wennberg, P. O.: Unexpected epoxide formation in the gas-phase photooxidation of isoprene, Science, 325, 730–733, 2009.

Peeters, J., Nguyen, T. L., and Vereecken, L.: HO_x radical regeneration in the oxidation of isoprene, Phys. Chem. Chem. Phys., 11, 5935–5939, 2009.

Perring, A. E., Bertram, T. H., Wooldridge, P. J., Fried, A., Heikes, B. G., Dibb, J., Crounse, J. D., Wennberg, P. O., Blake, N. J., Blake, D. R., Brune, W. H., Singh, H. B., and Cohen, R. C.: Airborne observations of total $RONO_2$: new constraints on the yield and lifetime of isoprene nitrates, Atmos. Chem. Phys., 9, 1451–1463, doi:10.5194/acp-9-1451-2009, 2009.

Pisso, I., Real, E., Law, K. S., Legras, B., Bousserez, N., Attie, J. L., and Schlager, H.: Estimation of mixing in the troposphere from Lagrangian trace gas reconstructions during longrange pollution plume transport, J. Geophys. Res.-Atmos., 114, D19301, doi:10.1029/2008JD011289, 2009.

Pollack, I. B., Lerner, B. M., and Ryerson, T. B.: Evaluation of ultraviolet light-emitting diodes for detection of atmospheric NO_2 by photolysis – chemiluminescence, J. Atmos. Chem., 65, 111–125, 2010.

Pöschl, U., von Kuhlmann, R., Poisson, N., and Crutzen, P.: Development and intercomparison of condensed isoprene oxidation mechanisms for global atmospheric modeling, J. Atmos. Chem., 37, 29–52, 2000.

Pugh, T. A. M., MacKenzie, A. R., Hewitt, C. N., Langford, B., Edwards, P. M., Furneaux, K. L., Heard, D. E., Hopkins, J. R., Jones, C. E., Karunaharan, A., Lee, J., Mills, G., Misztal, P., Moller, S., Monks, P. S., and Whalley, L. K.: Simulating atmospheric composition over a South-East Asian tropical rainforest: performance of a chemistry box model, Atmos. Chem. Phys., 10, 279–298, doi:10.5194/acp-10-279-2010, 2010.

Title Page

Abstract | Introduction

Conclusions | References

Tables | Figures

◀ | ▶

◀ | ▶

Back | Close

Full Screen / Esc

Printer-friendly Version

Interactive Discussion

Pugh, T. A. M., MacKenzie, A. R., Langford, B., Nemitz, E., Misztal, P. K., and Hewitt, C. N.: The influence of small-scale variations in isoprene concentrations on atmospheric chemistry over a tropical rainforest, Atmos. Chem. Phys., 11, 4121–4134, doi:10.5194/acp-11-4121-2011, 2011.

5   Pugh, T. A. M., Cain, M., Methven, J., Wild, O., Arnold, S. R., Real, E., Law, K. S., Emmerson, K. M., Owen, S. M., Pyle, J. A., Hewitt, C. N., and MacKenzie, A. R.: A Lagrangian model of air-mass photochemistry and mixing using a trajectory ensemble: the Cambridge Tropospheric Trajectory model of Chemistry And Transport (CiTTyCAT) version 4.2, Geosci. Model Dev., 5, 193–221, doi:10.5194/gmd-5-193-2012, 2012.

10   Real, E., Law, K. S., Weinzierl, B., Fiebig, M., Petzold, A., Wild, O., Methven, J., Arnold, S., Stohl, A., Huntrieser, H., Roiger, A., Schlager, H., Stewart, D., Avery, M., Sachse, G., Browell, E., Ferrare, R., and Blake, D.: Processes influencing ozone levels in Alaskan forest fire plumes during long-range transport over the North Atlantic, J. Geophys. Res.-Atmos., 112, D10S41, doi:10.1029/2006JD007576, 2007.

15   Real, E., Law, K. S., Schlager, H., Roiger, A., Huntrieser, H., Methven, J., Cain, M., Holloway, J., Neuman, J. A., Ryerson, T., Flocke, F., de Gouw, J., Atlas, E., Donnelly, S., and Parrish, D.: Lagrangian analysis of low altitude anthropogenic plume processing across the North Atlantic, Atmos. Chem. Phys., 8, 7737–7754, doi:10.5194/acp-8-7737-2008, 2008.

Rummel, U., Ammann, C., Kirkman, G. A., Moura, M. A. L., Foken, T., Andreae, M. O., and
20   Meixner, F. X.: Seasonal variation of ozone deposition to a tropical rain forest in southwest Amazonia, Atmos. Chem. Phys., 7, 5415–5435, doi:10.5194/acp-7-5415-2007, 2007.

Sillman, S. and He, D. Y.: Some theoretical results concerning O_3-NO_x-VOC chemistry and NO_x-VOC indicators, J. Geophys. Res., 107, 4659, doi:10.1029/2001JD001123, 2002.

Sitch, S., Cox, P. M., Collins, W. J., and Huntingford, C.: Indirect radiative forcing of climate
25   change through ozone effects on the land-carbon sink, Nature, 448, 791–794, 2007.

Squire, O. J., Archibald, A. T., Abraham, N. L., Beerling, D. J., Hewitt, C. N., Lathière, J., Pike, R. C., Telford, P. J., and Pyle, J. A.: Influence of future climate and cropland expansion on isoprene emissions and tropospheric ozone, Atmos. Chem. Phys., 14, 1011–1024, doi:10.5194/acp-14-1011-2014, 2014.

30   Squire, O. J., Archibald, A. T., Griffiths, P. T., Jenkin, M. E., Smith, D., and Pyle, J. A.: Influence of isoprene chemical mechanism on modelled changes in tropospheric ozone due to climate and land use over the 21st century, Atmos. Chem. Phys., 15, 5123–5143, doi:10.5194/acp-15-5123-2015, 2015.

Title Page

Abstract | Introduction

Conclusions | References

Tables | Figures

◀ | ▶

◀ | ▶

Back | Close

Full Screen / Esc

Printer-friendly Version

Interactive Discussion

Stone, D., Evans, M. J., Edwards, P. M., Commane, R., Ingham, T., Rickard, A. R., Brookes, D. M., Hopkins, J., Leigh, R. J., Lewis, A. C., Monks, P. S., Oram, D., Reeves, C. E., Stewart, D., and Heard, D. E.: Isoprene oxidation mechanisms: measurements and modelling of OH and HO_2 over a South-East Asian tropical rainforest during the OP3 field campaign, Atmos. Chem. Phys., 11, 6749–6771, doi:10.5194/acp-11-6749-2011, 2011.

Telford, P., Braesicke, P., Morgenstern, O., and Pyle, J.: Reassessment of causes of ozone column variability following the eruption of Mount Pinatubo using a nudged CCM, Atmos. Chem. Phys., 9, 4251–4260, doi:10.5194/acp-9-4251-2009, 2009.

Telford, P. J., Lathière, J., Abraham, N. L., Archibald, A. T., Braesicke, P., Johnson, C. E., Morgenstern, O., O'Connor, F. M., Pike, R. C., Wild, O., Young, P. J., Beerling, D. J., Hewitt, C. N., and Pyle, J.: Effects of climate-induced changes in isoprene emissions after the eruption of Mount Pinatubo, Atmos. Chem. Phys., 10, 7117–7125, doi:10.5194/acp-10-7117-2010, 2010.

Telford, P. J., Abraham, N. L., Archibald, A. T., Braesicke, P., Dalvi, M., Morgenstern, O., O'Connor, F. M., Richards, N. A. D., and Pyle, J. A.: Implementation of the Fast-JX Photolysis scheme (v6.4) into the UKCA component of the MetUM chemistry-climate model (v7.3), Geosci. Model Dev., 6, 161–177, doi:10.5194/gmd-6-161-2013, 2013.

Thompson, A., Witte, J., McPeters, R., Oltmans, S., Schmidlin, F., Logan, J., Fujiwara, M., Kirchhoff, V., Posny, F., Coetzee, G., Hoegger, B., Kawakami, S., Ogawa, T., Johnson, B., Vomel, H., and Labow, G.: Southern Hemisphere Additional Ozonesondes (SHADOZ) 1998–2000 tropical ozone climatology – 1. Comparison with Total Ozone Mapping Spectrometer (TOMS) and ground-based measurements, J. Geophys. Res., 108, 8238, doi:10.1029/2001JD000967, 2003.

UNECE: Mapping Manual: UNECE Convention on Long-range Transboundary Air Pollution. Chapter III Mapping Critical Levels for Vegetation, 52, 2010.

Wild, O., Law, K. S., McKenna, D. S., Bandy, B. J., Penkett, S. A., and Pyle, J. A.: Photochemical trajectory modeling studies of the North Atlantic region during August 1993, J. Geophys. Res., 101, 29269–29288, 1996.

WHO: Air Quality Guidelines for Europe, Tech. Rep., World Health Organization, Copenhagen, Denmark, 2000.

WMO: Scientific assessment of ozone depletion: 1995 Global Ozone Research and Monitoring Project, Geneva, Switzerland, 1995.

Title Page

Abstract | Introduction

Conclusions | References

Tables | Figures

|◀ | ▶|

◀ | ▶

Back | Close

Full Screen / Esc

Printer-friendly Version

Interactive Discussion

Yienger, J. J. and Levy II, H.: Global inventory of soil-biogenic NO$_x$ emissions, J. Geophys. Res., 100, 11447–11464, 1995.

Title Page

Abstract | Introduction

Conclusions | References

Tables | Figures

◄ | ►

◄ | ►

Back | Close

Full Screen / Esc

Printer-friendly Version

Interactive Discussion

Table 1. Parameters subject to which mixing is explored in formulations, Mix1–3: κ_{FT} and κ_{BL} are free-troposphere and boundary-layer diffusion coefficients; D is a free tropospheric depth parameter. τ_{FT} and τ_{BL} are the resulting free-troposphere and boundary-layer relaxation timescales, the latter when subject to a boundary layer height (BL height) of 1000 m.

Formulation	κ_{FT} $(m^2\,s^{-1})$	κ_{BL} $(m^2\,s^{-1})$	D (m)	τ_{FT} (h)	τ_{BL} (h)
Mix1	1.5	15.0	200	3.7	9.3
Mix2	0.5	5.0	200	11.1	27.8
Mix3	0.5	5.0	500	69.4	27.8

Table 2. Main features of the eight CiTTyCAT model setups, including: the UM-UKCA integration used to initialise the composition of air parcels; the chemical mechanism employed; the trace gas emissions used; and the inclusion, or otherwise, of mixing subject to formulations Mix1–3.

CiTTyCAT model setup	Initialisation	Chemistry	Emissions	Mixing
1. CiTTyCAT (CheT)	UM-UKCA (CheT)	CheT	UKCA res	None
2. CiTTyCAT (CheT2)	UM-UKCA (CheT2)	CheT2	UKCA res	None
3. CiTTyCAT (CheT, HRE)	UM-UKCA (CheT)	CheT	High res	None
4. CiTTyCAT (CheT2, HRE)	UM-UKCA (CheT2)	CheT2	High res	None
5. CiTTyCAT (CheT, Mix1–3)	UM-UKCA (CheT)	CheT	UKCA res	Mix1–3
6. CiTTyCAT (CheT2, Mix1–3)	UM-UKCA (CheT2)	CheT2	UKCA res	Mix1–3
7. CiTTyCAT (CheT, HRE, Mix1–3)	UM-UKCA (CheT)	CheT	High res	Mix1–3
8. CiTTyCAT (CheT2, HRE, Mix1–3)	UM-UKCA (CheT2)	CheT2	High res	Mix1–3

Table 3. Global trace gas emission totals (employed in all integrations), including the total anthropogenic and biogenic contributions.

Tg (species) yr^{-1}	NO_2	CO	HCHO	C_2H_6	C_3H_8	$CH_3C(O)CH_3$	CH_3CHO	C_5H_8
Anthropogenic	99.0	875	2.37	9.85	9.46	4.35	6.54	0.0
Biogenic	17.8	0.0	4.21	0.0	0.0	39.4	14.3	401
Total	117	875	6.57	9.85	9.46	43.7	20.8	401

Title Page

Abstract | Introduction

Conclusions | References

Tables | Figures

Back | Close

Full Screen / Esc

Printer-friendly Version

Interactive Discussion

Table 4. Metrics regarding the [O_3] simulated downwind of Manaus in UM-UKCA and CiTTy-CAT, subject to CheT and CheT2 chemical mechanisms; all integrations with CiTTyCAT employ mixing formulation Mix3, and those labelled "HRE" employ High res emissions. See text for a discussion of the accumulation time for the reported AOT40-like metric, labelled "AOT40".

Simulated [O_3] metric	UM-UKCA		CiTTyCAT (Mix3)			
	CheT	CheT2	CheT, HRE	CheT2, HRE	CheT	CheT2
No. of times [O_3] > 50 ppbv	0	0	5	5	4	5
Mean [O_3] (ppbv)	32.5	32.5	35.1	35.9	35.0	36.0
Increase in mean [O_3]	–	–	2.6 ppbv	3.4 ppbv	2.5 ppbv	3.5 ppbv
relative to UM-UKCA	–	–	+8 %	+11 %	+8 %	+11 %
(subject to same chemistry)						
"AOT40" (ppbv h)	22.6	17.5	863	1081	889	1091
Increase in "AOT40"	–	–	841 ppbv h	1063 ppbv h	866 ppbv h	1073 ppbv h
relative to UM-UKCA	–	–	38×	62×	39×	62×
(subject to same chemistry)						
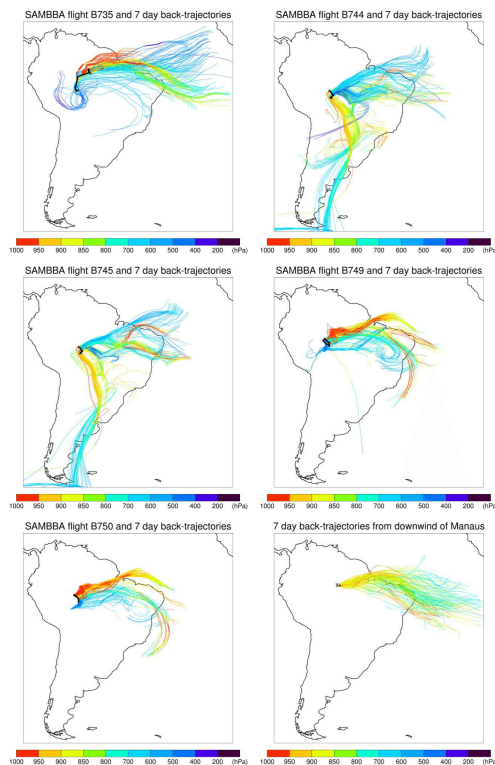
Figure 1. Flight tracks (black lines), and 7 day back-trajectories arriving on these at one minute intervals (coloured according to pressure), for SAMBBA flights B735, B744, B745, B749 and B750; see text for details. Bottom right: 7 day back-trajectories arriving at a site roughly 100 km downwind (1° west) of Manaus at 6 hourly intervals throughout September 2012 (coloured according to pressure); "×" marks the site (61.0° W, 3.1° S) and the black dot marks Manaus.
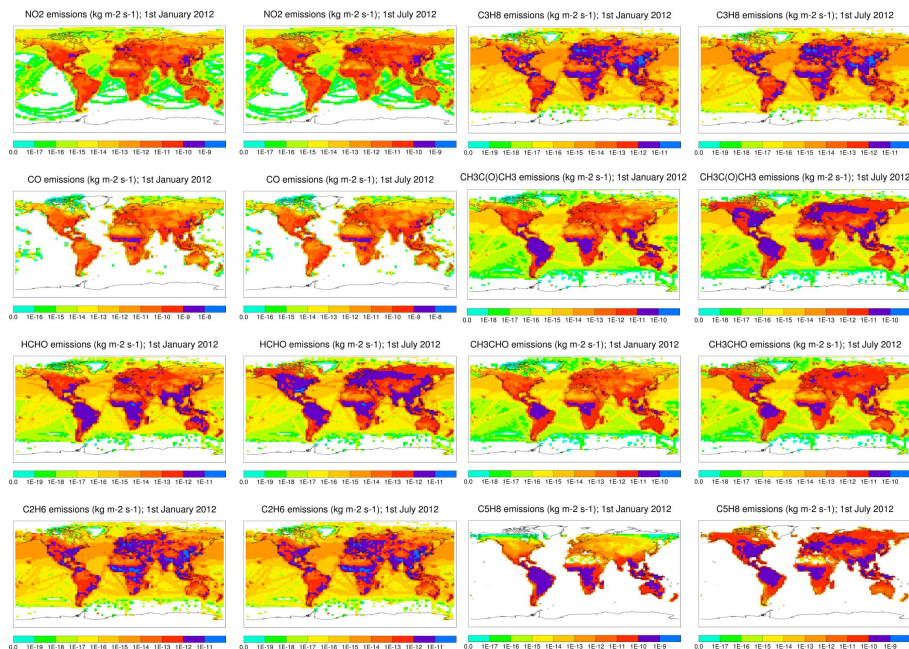
Figure 2. Total (anthropogenic + biogenic) trace gas emissions at 3.75° longitude × 2.5° latitude on 1 January and 1 July 2012, employed in UM-UKCA (run in "climate mode") and "UKCA res" integrations with CiTTyCAT.

Full Screen / Esc

Printer-friendly Version

Interactive Discussion
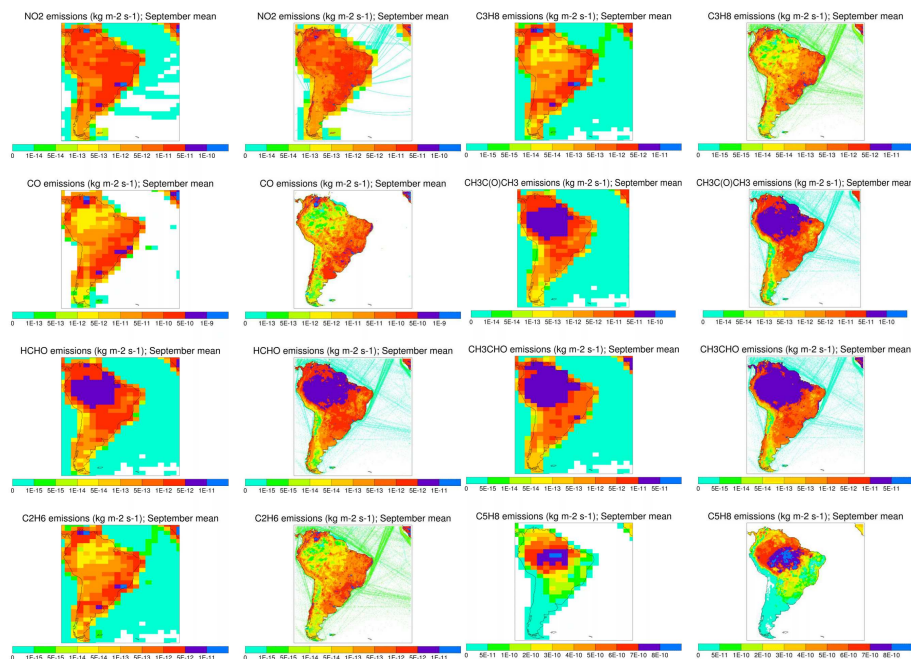
Figure 3. Total (anthropogenic + biogenic) trace gas emissions employed in CiTTyCAT "UKCA res" integrations (left) and "High res" integrations (right); all emissions are September 2012 monthly means, focussing on South America.
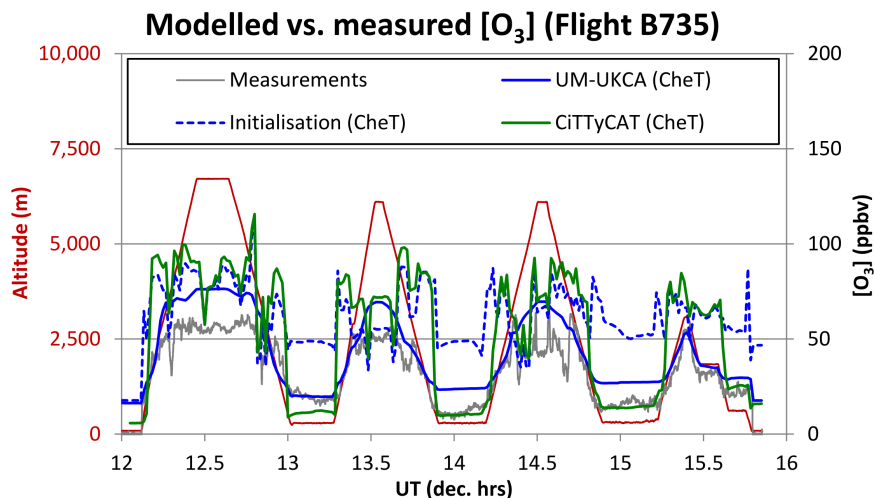
Figure 4. [O_3] measured on SAMBBA flight B735 and simulated in UM-UKCA (CheT) and CiTTyCAT (CheT). The [O_3] with which CiTTyCAT is initialised is also illustrated; see text for details.
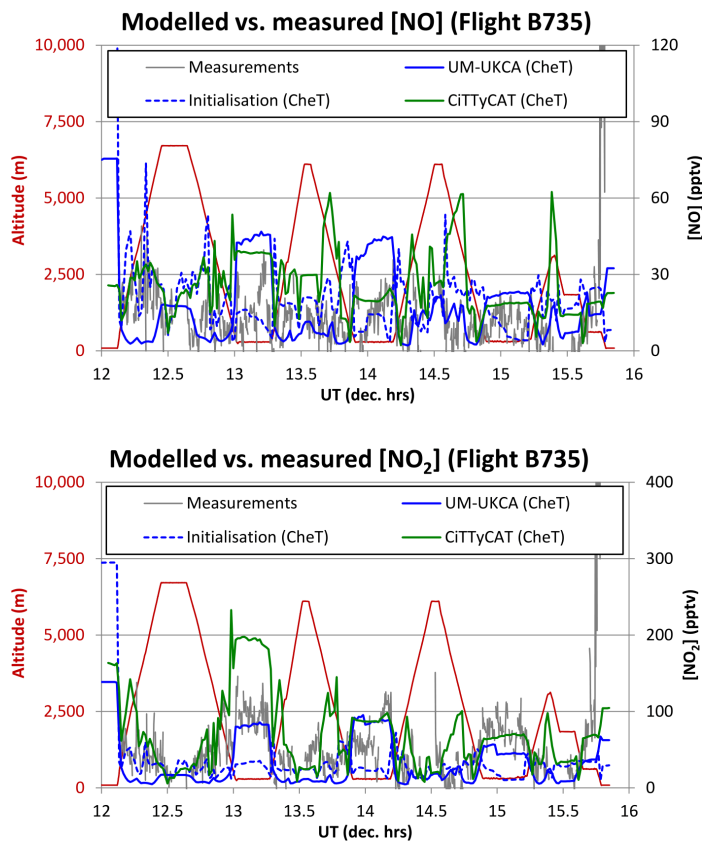
Figure 5. [NO] and [NO$_2$] measured on SAMBBA flight B735 and simulated in UM-UKCA (CheT) and CiTTyCAT (CheT). The [NO] and [NO$_2$] with which CiTTyCAT is initialised are also illustrated; see text for details.
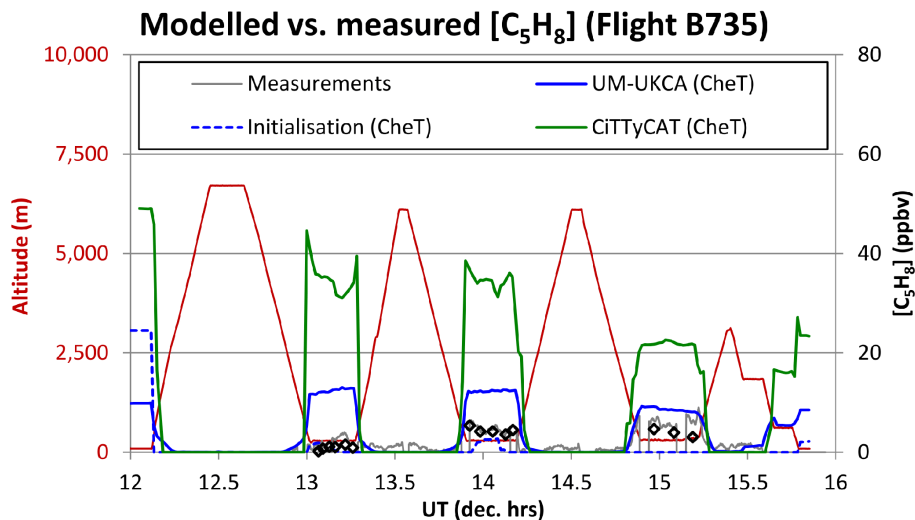
Figure 6. [C_5H_8] measured on SAMBBA flight B735 and simulated in UM-UKCA (CheT) and CiTTyCAT (CheT). The [C_5H_8] with which CiTTyCAT is initialised is also illustrated; the open black diamonds correspond to the [C_5H_8] measurements based on whole air samples.

Figure 7. [CO] measured on SAMBBA flight B735 and simulated in UM-UKCA (CheT) and CiTTyCAT (CheT). The [CO] with which CiTTyCAT is initialised is also illustrated; see text for details.
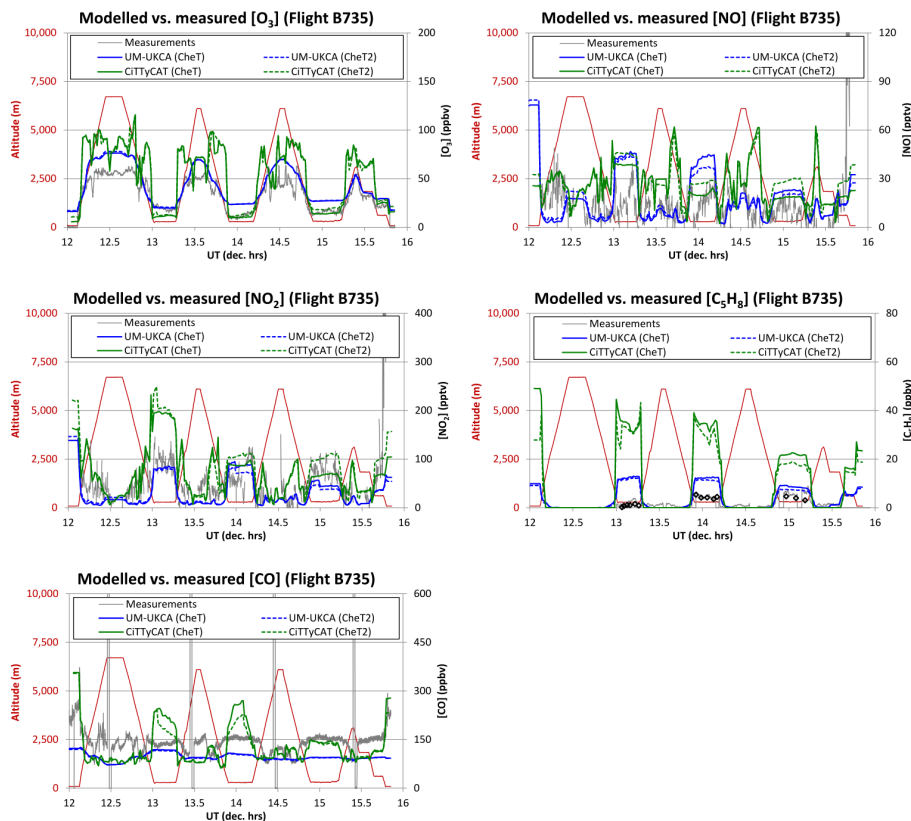
Figure 8. [O_3], [NO], [NO_2], [C_5H_8] and [CO] measured on SAMBBA flight B735 and simulated in UM-UKCA and CiTTyCAT, subject to CheT and CheT2 chemical mechanisms (see Sect. 2.3 for more details); the open black diamonds correspond to [C_5H_8] measurements based on whole air samples.

Isoprene chemistry in pristine and polluted Amazon environments

J. G. Levine et al.
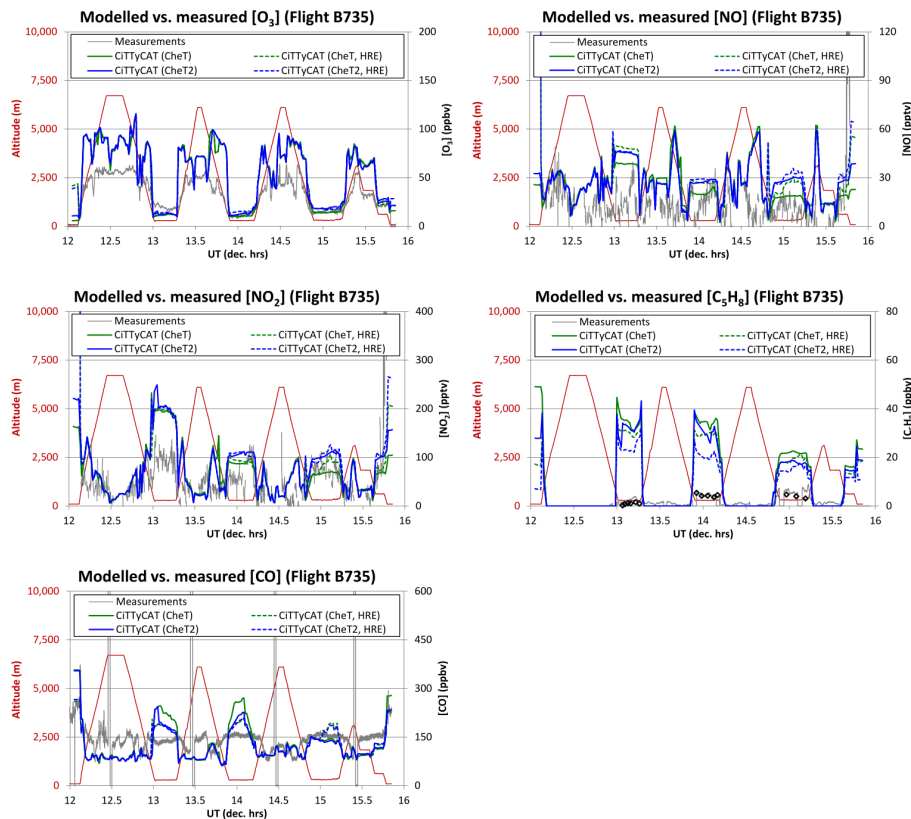
Figure 9. [O_3], [NO], [NO_2], [C_5H_8] and [CO] measured on SAMBBA flight B735 and simulated in CiTTyCAT, subject to CheT and CheT2 chemical mechanisms (see Sect. 2.3) and both "UKCA res" emissions and "High res" emissions (HRE; see Sect. 2.4 for more details); the open black diamonds correspond to [C_5H_8] measurements based on whole air samples.
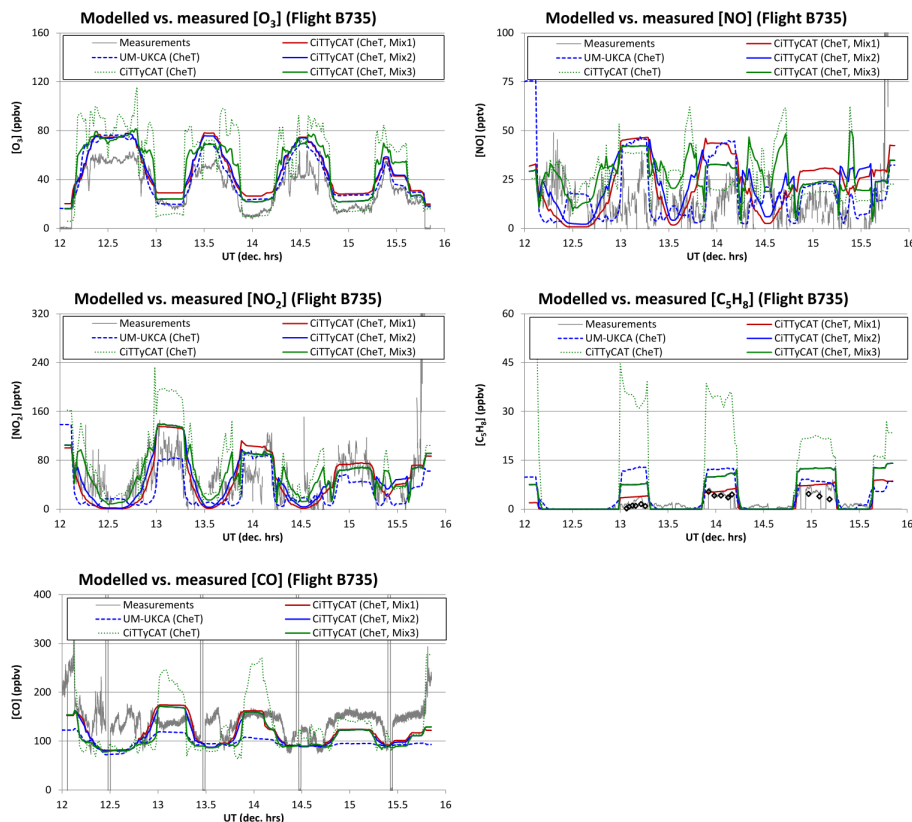
Figure 10. [O$_3$], [NO], [NO$_2$], [C$_5$H$_8$] and [CO] measured on SAMBBA flight B735 and simulated in UM-UKCA (CheT) and CiTTyCAT (CheT), the latter subject to no mixing and, subsequently, three formulations of simple diffusive vertical mixing (relaxation towards background values) as outlined in Sect. 2.2.2 and Table 1; the open black diamonds correspond to [C$_5$H$_8$] measurements based on whole air samples.

Title Page

Abstract   Introduction

Conclusions   References

Tables   Figures

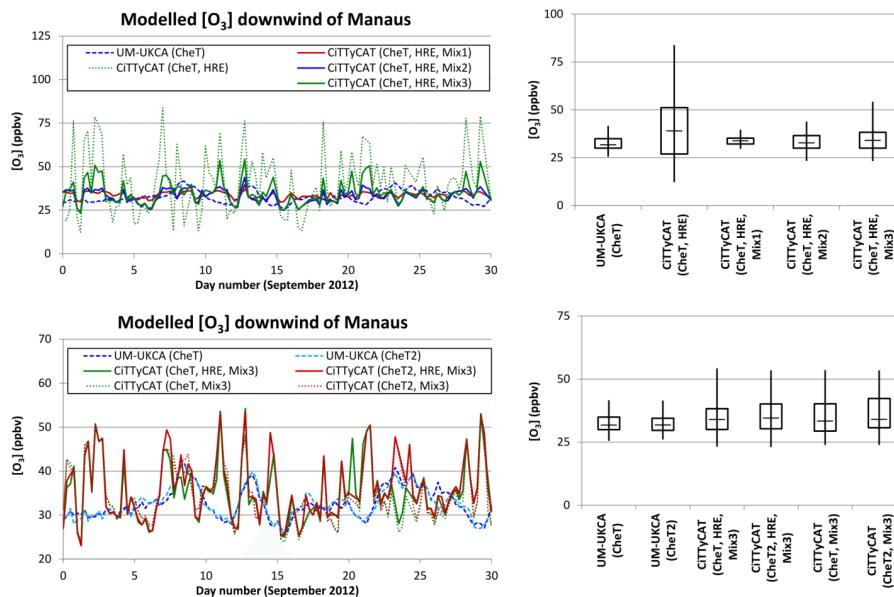◄   ►|

◄   ►

Back   Close

Full Screen / Esc

Printer-friendly Version

Interactive Discussion

Figure 11. Left: [O_3] simulated approximately 100 km downwind of Manaus in UM-UKCA and CiTTyCAT; the top panel compares CiTTyCAT integrations, all employing the CheT chemical mechanism but differing with respect to mixing formulation (Mix1–3; see Sect. 2.2.2 and Table 1 for more details), whilst the bottom panel compares CiTTyCAT integrations, all employing mixing formulation, Mix3, but differing with respect to the chemical mechanism (CheT or CheT2) and/or the resolution of trace gas emissions employed (HRE = High res ems). Right: the corresponding "box and whisker" plots of the minimum, maximum, median, and first- and third quartile [O_3] values. The UM-UKCA (CheT) and CiTTyCAT (CheT, HRE, Mix3) runs are included in both top and bottom panels.

Title Page

Abstract   Introduction

Conclusions   References

Tables   Figures

|◄   ►|

◄   ►

Back   Close

Full Screen / Esc

Printer-friendly Version

Interactive Discussion